

FILE COPY
NO. 8

NATIONAL ADVISORY COMMITTEE FOR AERONAUTICS

REPORT No. 758

PERFORMANCE OF NACA EIGHT-STAGE AXIAL-FLOW COMPRESSOR DESIGNED ON THE BASIS OF AIRFOIL THEORY

By JOHN T. SINNETTE, Jr., OSCAR W. SCHEY, and J. AUSTIN KING

THIS DOCUMENT ON LOAN FROM THE FILES OF



NATIONAL ADVISORY COMMITTEE FOR AERONAUTICS
LANGLEY AERONAUTICAL LABORATORY
LANGLEY FIELD, HAMPTON, VIRGINIA

RETURN TO THE ABOVE ADDRESS.

REQUESTS FOR PUBLICATIONS SHOULD BE ADDRESSED
AS FOLLOWS:

NATIONAL ADVISORY COMMITTEE FOR AERONAUTICS 1943
1724 I STREET, N.W.,
WASHINGTON 25, D.C.

AERONAUTIC SYMBOLS

1. FUNDAMENTAL AND DERIVED UNITS

Symbol		Metric		English	
		Unit	Abbreviation	Unit	Abbreviation
Length	<i>l</i>	meter	m	foot (or mile)	ft (or mi)
Time	<i>t</i>	second	s	second (or hour)	sec (or hr)
Force	<i>F</i>	weight of 1 kilogram	kg	weight of 1 pound	lb
Power	<i>P</i>	horsepower (metric)		horsepower	hp
Speed	<i>V</i>	{kilometers per hour meters per second}	kph mps	{miles per hour feet per second}	mph fps

2. GENERAL SYMBOLS

<i>W</i>	Weight = mg	<i>v</i>	Kinematic viscosity
<i>g</i>	Standard acceleration of gravity = 9.80665 m/s^2 or 32.1740 ft/sec^2	ρ	Density (mass per unit volume)
<i>m</i>	Mass = $\frac{W}{g}$		Standard density of dry air, $0.12497 \text{ kg-m}^{-3}\text{s}^2$ at 15° C and 760 mm; or $0.002378 \text{ lb-ft}^{-4} \text{ sec}^2$
<i>I</i>	Moment of inertia = mk^2 . (Indicate axis of radius of gyration <i>k</i> by proper subscript.)		Specific weight of "standard" air, 1.2255 kg/m^3 or 0.07651 lb/cu ft
μ	Coefficient of viscosity		

3. AERODYNAMIC SYMBOLS

<i>S</i>	Area	i_w	Angle of setting of wings (relative to thrust line)
S_w	Area of wing	i_t	Angle of stabilizer setting (relative to thrust line)
<i>G</i>	Gap	<i>Q</i>	Resultant moment
<i>b</i>	Span	Ω	Resultant angular velocity
<i>c</i>	Chord	<i>R</i>	Reynolds number, $\rho \frac{Vl}{\mu}$ where <i>l</i> is a linear dimension (e.g., for an airfoil of 1.0 ft chord, 100 mph, standard pressure at 15° C , the corre- sponding Reynolds number is 935,400; or for an airfoil of 1.0 m chord, 100 mps, the corre- sponding Reynolds number is 6,865,000)
<i>A</i>	Aspect ratio, $\frac{b^2}{S}$	α	Angle of attack
<i>V</i>	True air speed	ϵ	Angle of downwash
<i>q</i>	Dynamic pressure, $\frac{1}{2} \rho V^2$	α_0	Angle of attack, infinite aspect ratio
<i>L</i>	Lift, absolute coefficient $C_L = \frac{L}{qS}$	α_i	Angle of attack, induced
<i>D</i>	Drag, absolute coefficient $C_D = \frac{D}{qS}$	α_a	Angle of attack, absolute (measured from zero- lift position)
D_0	Profile drag, absolute coefficient $C_{D_0} = \frac{D_0}{qS}$	γ	Flight-path angle
D_i	Induced drag, absolute coefficient $C_{D_i} = \frac{D_i}{qS}$		
D_p	Parasite drag, absolute coefficient $C_{D_p} = \frac{D_p}{qS}$		
<i>C</i>	Cross-wind force, absolute coefficient $C_c = \frac{C}{qS}$		

REPORT No. 758

PERFORMANCE OF NACA EIGHT-STAGE AXIAL-FLOW COMPRESSOR DESIGNED ON THE BASIS OF AIRFOIL THEORY

By JOHN T. SINNETTE, Jr., OSCAR W. SCHEY, and J. AUSTIN KING

**Aircraft Engine Research Laboratory
Cleveland, Ohio**

National Advisory Committee for Aeronautics

Headquarters, 1500 New Hampshire Avenue NW., Washington 25, D. C.

Created by act of Congress approved March 3, 1915, for the supervision and direction of the scientific study of the problems of flight (U. S. Code, title 49, sec. 241). Its membership was increased to 15 by act approved March 2, 1929. The members are appointed by the President, and serve as such without compensation.

JEROME C. HUNSAKER, Sc. D., Cambridge, Mass., *Chairman*

LYMAN J. BRIGGS, Ph. D., *Vice Chairman*, Director, National Bureau of Standards.

JOHN C. McCAIN, Rear Admiral, United States Navy, Deputy Chief of Operations (Air), Navy Department.

CHARLES G. ABBOT, Sc. D., *Vice Chairman*, *Executive Committee*, Secretary, Smithsonian Institution.

GEORGE J. MEAD, Sc. D., Washington, D. C.

HENRY H. ARNOLD, General, United States Army, Commanding General, Army Air Forces, War Department.

ERNEST M. PACE, Rear Admiral, United States Navy, Special Assistant to Chief of Bureau of Aeronautics, Navy Department.

WILLIAM A. M. BURDEN, Special Assistant to the Secretary of Commerce.

FRANCIS W. REICHELDERFER, Sc. D., Chief, United States Weather Bureau.

VANNEVAR BUSH, Sc. D., Director, Office of Scientific Research and Development, Washington, D. C.

EDWARD WARNER, Sc. D., Civil Aeronautics Board, Washington, D. C.

WILLIAM F. DURAND, Ph. D., Stanford University, California.

ORVILLE WRIGHT, Sc. D., Dayton, Ohio.

OLIVER P. ECHOLS, Major General, United States Army, Chief of Maintenance, Matériel, and Distribution, Army Air Forces, War Department.

THEODORE P. WRIGHT, Sc. D., Assistant Chief, Aircraft Branch, War Production Board.

GEORGE W. LEWIS, Sc. D., *Director of Aeronautical Research*

JOHN F. VICTORY, LL.M., *Secretary*

HENRY J. E. REID, Sc. D., Engineer-in-Charge, Langley Memorial Aeronautical Laboratory, Langley Field, Va.

SMITH J. DEFANCE, B. S., Engineer-in-Charge, Ames Aeronautical Laboratory, Moffett Field, Calif.

EDWARD R. SHARP, LL.B., Manager, Aircraft Engine Research Laboratory, Cleveland Airport, Cleveland, Ohio

CARLTON KEMPER, B. S., Executive Engineer, Aircraft Engine Research Laboratory, Cleveland Airport, Cleveland, Ohio

TECHNICAL COMMITTEES

AERODYNAMICS

AIRCRAFT STRUCTURES

POWER PLANTS FOR AIRCRAFT

OPERATING PROBLEMS

AIRCRAFT MATERIALS

JET PROPULSION

Coordination of Research Needs of Military and Civil Aviation

Preparation of Research Programs

Allocation of Problems

Prevention of Duplication

LANGLEY MEMORIAL AERONAUTICAL LABORATORY
Langley Field, Va.

AMES AERONAUTICAL LABORATORY
Moffett Field, Calif.

AIRCRAFT ENGINE RESEARCH LABORATORY, Cleveland Airport, Cleveland, Ohio

Conduct, under unified control, for all agencies, of scientific research on the fundamental problems of flight

OFFICE OF AERONAUTICAL INTELLIGENCE, Washington, D. C.

Collection, classification, compilation, and dissemination of scientific and technical information on aeronautics

REPORT No. 758

PERFORMANCE OF NACA EIGHT-STAGE AXIAL-FLOW COMPRESSOR DESIGNED ON THE BASIS OF AIRFOIL THEORY

By JOHN T. SINNETTE, Jr., OSCAR W. SCHEY, and J. AUSTIN KING

SUMMARY

The NACA has conducted an investigation to determine the performance that can be obtained from a multistage axial-flow compressor based on airfoil research. A theory was developed; an eight-stage axial-flow compressor was designed, constructed, and tested.

The design basis for each stage was a symmetrical velocity diagram and an axial component of velocity constant with respect to the radius. The rotor was sufficiently tapered to produce an increase in axial velocity from the inlet to the outlet of the compressor. The stator had a constant inside diameter of 14 inches. A row of entrance guide vanes reduced the relative velocity at the entrance of the first row of rotor blades. The limiting condition used in the design of the blades were a relative velocity of 0.7 the local velocity of sound, a lift coefficient of 0.7, and a solidity of approximately 1.2.

The performance of the compressor was determined for speeds from 5000 to 14,000 rpm with varying air flow at each speed. Most of the tests were made with some cooling of the inlet air, but a few were made with air at room temperature. The performance was determined in accordance with the Committee's recommended procedure for testing superchargers.

The NACA eight-stage axial-flow compressor without lagging gave an adiabatic temperature-rise efficiency of 87 percent at a pressure ratio of 3.42 and an inlet volume flow of 129 cubic feet per second. The expected performance was obtained, showing that a multistage compressor of high efficiency can be designed by the application of airfoil theory.

INTRODUCTION

Interest in axial-flow compressors has greatly increased since 1935 as a result of efforts to obtain compressors of high efficiency for application to combustion-gas turbine units and aircraft-engine superchargers. In the combustion-gas turbine, where a large excess quantity of air is compressed for cooling the products of combustion to a temperature allowable in the turbine, the efficiency of compression is of utmost importance; in engine supercharging, the need for high efficiency has steadily risen with the increasing demand for high-altitude performance and the trend toward higher manifold pressures for increased power.

The combustion-gas turbine unit, especially in its adaptation to the jet-propulsion engine, requires a compressor of high flow capacity. For aircraft application, the over-all diameter of such units should be kept to a minimum because

the drag on an airplane increases with the frontal area required for the power plant. The axial-flow compressor, at present, is unexcelled in its capacity to deliver maximum air flow for a given over-all diameter; the ultimate possible mass flow is obtained when the inlet velocity equals the velocity of sound.

Based on the original proposal of Burdin formulated as early as 1847, the fundamental principles of multistage axial-flow compressors and turbines were clearly presented by Tournaire in 1853 in a paper submitted to the French Academie des Sciences (reference 1, pp. 14, 20). Stolze used an axial-flow compressor in a combustion-gas turbine unit designed about 1872 and tested between 1900 and 1904, but was unable to obtain useful work from the turbine because of the inefficiency of the compressor (reference 1, pp. 23 and 24, and reference 2). The Parson Co. of England built about 30 axial-flow compressors between 1900 and 1908, the largest of which had a capacity of 50,000 cubic feet per minute, but finally abandoned this type of compressor because the efficiencies obtained were not comparable with those of the centrifugal compressor introduced commercially in 1908 (references 2 and 3).

Research on axial-flow compressors was discouraged by these early unsuccessful attempts to obtain acceptable efficiencies. With the development of airfoil theory and its extension to airfoil cascades, the successful application of aerodynamic principles to propellers, windmills, fans, turbines, and pumps resulted in renewed effort to develop efficient axial-flow compressors. By 1938, as a result of extensive theoretical and experimental research (references 4 to 19), a number of designers had been able to obtain efficiencies of 75 to 85 percent with axial-flow fans (references 4, 12, 15, 16, 17, and 20 to 24). Because these efficiencies were appreciably higher than those obtained with centrifugal compressors, the possibilities of multistage axial-flow compressors appeared highly promising. An account of a multistage axial-flow compressor with an efficiency comparable with that of the best centrifugal compressors was published in 1935 (reference 25) in the description of a Velox steam generator. This compressor had an efficiency "of the order of 73 percent." Extensive investigations relating to axial-flow compressors have been made since that time (references 26 to 32).

The NACA recognized that high-efficiency compressors could be designed by the application of aerodynamic principles. In 1938 Eastman N. Jacobs of the Aerodynamic

Division and Eugene W. Wasielewski of the Power Plants Division at Langley Memorial Aeronautical Laboratory began an investigation at Langley Field, Va., for the purpose of determining the performance of an axial-flow compressor based on the current information gained from extensive research on airfoils. A theory was developed and applied to the design and construction of an eight-stage compressor and preliminary tests were conducted. For the present report, the compressor was tested over a range of speeds from 5000 to 14,000 rpm, and a range of air flows from full throttle to surge for each speed except the highest speeds at which the flow was limited because of insufficient power. Heat-transfer tests were made with and without lagging of the compressor. Most of the tests were made with some refrigeration of the inlet air, but a few were made at room temperature. This investigation was conducted at the NACA Langley laboratory during 1941 and 1942.

The General Electric Co. gave valuable assistance in making the tests, particularly in designing and constructing the journal and thrust bearings that replaced the original roller and ball bearings.

THE NACA AXIAL-FLOW COMPRESSOR

CONSTRUCTION

The principal mechanical features of the NACA axial-flow compressor are shown in figures 1, 2, and 3. The compressor essentially consists of a solid rotor enclosed in a casing of three sections: the bellmouthed inlet, the cylindrical stator, and the scroll collector. Each section of the casing is divided along the median horizontal plane to permit removal of the upper half as a unit (figs. 1, 2, and 3). The maximum diameter of the compressor at the inlet is approximately 20 inches and the over-all length is approximately 42 inches. Compression of the air is accomplished by eight stages; each of the eight stages consists of a row of rotor blades followed by a row of stator blades. A row of entrance guide vanes mounted in the stator precedes the first row of rotor blades.

The entire casing and the supports of the compressor were cast from aluminum alloy. The front bearing housing and compressor support were cast integral with the inlet section; the rear bearing housing and support were cast integral with the collector section. The streamlined front bearing housing is supported by six streamlined struts that are drilled for the oil supply and drain. The stator was machined to an inside diameter of 14 inches and ribbed for stiffness (fig. 1). Holes were accurately machined in the stator for mounting the entrance guide vanes and the eight rows of stator blades (fig. 3). The annular diffuser passage into the scroll collector, the collector proper, and the 8-inch tangential discharge opening make up the collector section. The cross-sectional area of the collector increases until the maximum area is reached at the discharge opening.

In order to obtain maximum strength and high critical speeds, the rotor and the bearing shafts were machined as a solid, integral unit from a duralumin forging of high physical properties. The shape of the rotor and of the flow passages through the compressor are shown in figures 1 and 2. The

holes for mounting the rotor blades were precisely machined to make the blade bases flush with the rotor surface at the design blade setting.

The rotor was originally mounted on "ultraprecision" ball and roller bearings; the radial load was carried by two roller bearings each on the front and on the rear; the thrust load was carried by two ball bearings on the rear. The rear bearings repeatedly gave trouble at speeds of 11,000 rpm or less from overheating caused, in part, by heat transferred from the discharge air to the bearing housing. After several unsuccessful attempts to cool the bearings and after two bearing failures, the entire bearing installation was replaced by special journal and fixed-wedge thrust bearings, similar to steam-turbine bearings, designed and constructed by the General Electric Co. The journal bearings were self-aligning and had a system of circumferential and axial grooves and an oil dam on the bearing surface to control the oil film and prevent shaft whirling (reference 33). The thrust bearing was mounted on the rear end of the compressor. Hardened-and-ground-steel sleeves were pressed on the duralumin shafts to provide a good bearing surface. This bearing installation proved very satisfactory even at the maximum speed of 14,000 rpm used in these tests.

For both bearing installations, the front and the rear bearings were lubricated through separate systems; suction on the oil drains was used to prevent oil from being drawn into the air stream. When the ball and roller bearings were used, a drip system was provided to supply sufficient oil for mist lubrication. For the journal- and thrust-bearing installation, a forced feed was used with a differential pressure across the bearings of approximately 30 pounds. About 1 gallon of oil per minute flowed through the front journal bearing and about 14 gallons per minute flowed through the rear journal and thrust bearings. Pressure cut-off switches were installed to stop the dynamometers if the oil pressure dropped too low.

The blades were made from forged 24S-T duralumin bar stock, which has especially desirable physical properties at high temperatures. Each blade consists of an airfoil section, a base flush with the wall at the design blade setting, and a mounting shank. The stator blades were body-fitted in the stator holes and secured with nuts and lock washers; the rotor blades were screwed into the rotor and prevented from turning by the friction locks at the end of the shanks (fig. 1). This method of construction and mounting permits changing the angle setting of all blades within limits determined by the blade-tip clearances. Any adjustment, however, would cause slight irregularities at the blade bases, which are flush only at design settings. Small irregularities at the tips and the bases of the blades can be corrected by scraping.

The untapered rotor and stator blades were designed with the thickness distribution of the NACA 0009-34 airfoil section (reference 34) and with a maximum camber of 5.4 percent of the chord. Instead of using a standard airfoil section for the entrance guide vanes, the space between the vanes was considered to be a passage and the vanes were curved to give the desired prerotation to the air. The coordinates of the blades and the vanes are given in table I.

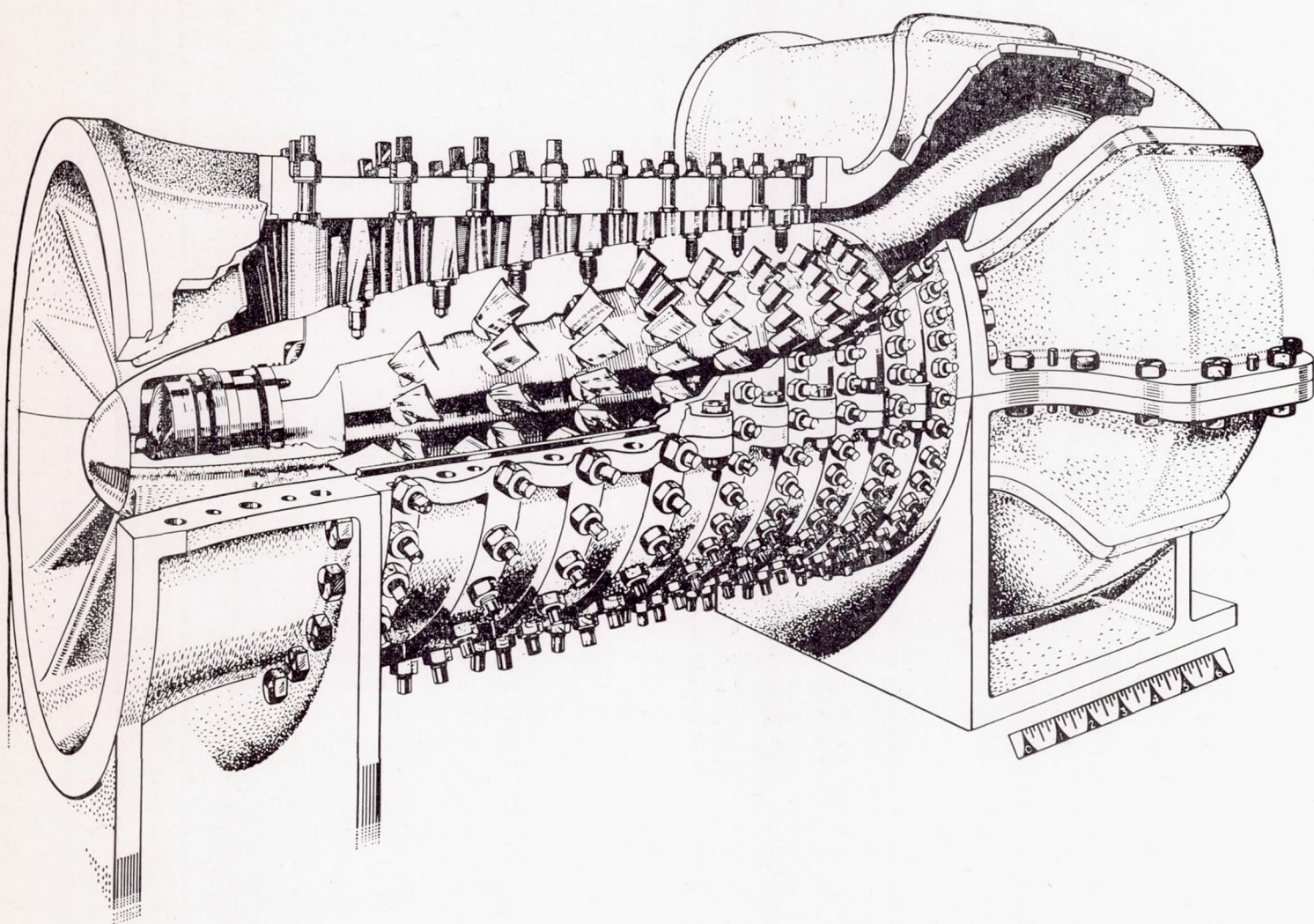


FIGURE 1.—NACA eight-stage axial-flow compressor.

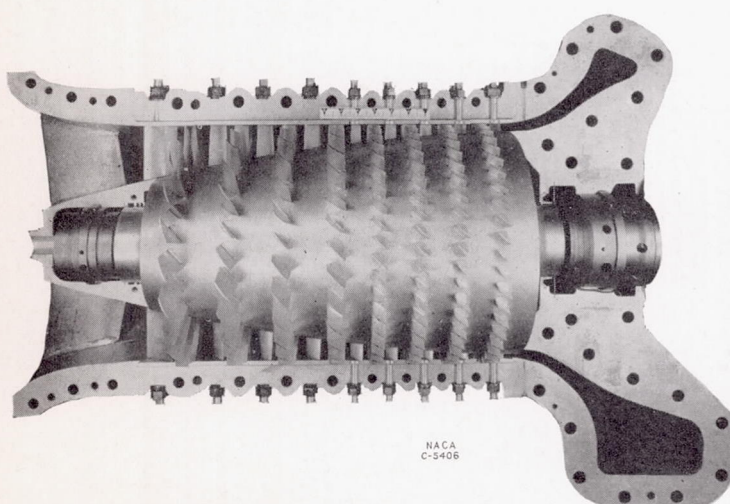


FIGURE 2.—NACA eight-stage axial-flow compressor with upper half of casing removed.

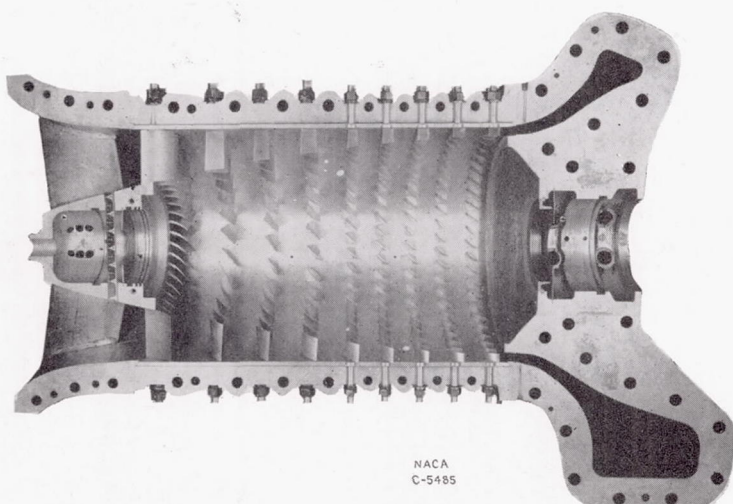


FIGURE 3.—Lower half of casing showing entrance guide vanes, stator blades, and section of scroll collector.

TABLE I.—SECTION COORDINATES OF ROTOR AND STATOR BLADES AND GUIDE VANES IN PERCENTAGE OF CHORD

[The reference chord of the guide vane is from the center of curvature of the leading edge to the trailing edge; the leading-edge radius is 0.80 percent of the chord. The leading-edge radius of the rotor and the stator blades is 0.22 percent of the chord.]

Rotor and stator blades				Entrance guide vanes		
Upper surface		Lower surface		Station	Upper-surface ordinate	Lower-surface ordinate
Station	Ordinate	Station	Ordinate			
0.00	0.00	0.00	0.00	0.00	1.05	-0.80
1.03	1.23	1.47	-.41	1.94	2.14	-.45
2.21	1.96	2.79	-.49	3.94	3.34	.00
4.64	3.13	5.36	-.54	9.87	6.33	1.35
7.10	4.11	7.90	-.52	16.79	9.12	2.74
9.58	4.94	10.42	-.47	23.82	11.31	3.99
14.58	6.36	15.42	-.33	30.79	12.90	4.98
19.61	7.45	20.39	-.15	38.71	14.00	5.98
29.73	8.95	30.27	.27	45.74	14.40	6.63
39.88	9.68	40.12	.69	51.72	14.30	7.03
50.04	9.76	49.96	1.02	57.75	13.70	7.22
60.19	9.23	59.81	1.26	63.78	12.86	7.13
70.30	8.05	69.70	1.35	70.85	11.46	6.63
80.38	6.13	79.62	1.20	76.78	9.97	5.93
90.28	3.31	89.72	.56	82.81	7.97	4.83
95.16	1.68	94.84	.18	88.79	5.63	3.49
100.00	.09	100.00	-.09	94.97	2.74	1.69
				100.00	0.00	0.00

The clearance between adjacent rows of rotor blades varies from approximately $\frac{1}{2}$ inch between the first two rows to approximately $\frac{3}{16}$ inch between the last two rows. The fillets at the root of the blades were kept very small to avoid disturbing the flow around the root of the blades; the fillet radius on the small blades is 0.015 inch and on the large blades, 0.025 inch. The stationary blade-tip clearance is approximately 0.015 inch. The blades in the first rotor have a uniform twist of $11\frac{1}{4}^\circ$ per inch and all other rotor blades have a uniform twist of $6\frac{1}{4}^\circ$ per inch. The stator blades have a

uniform twist of $5\frac{3}{4}^\circ$ per inch. The inlet guide vanes are not twisted. The number of blades in each row, the chord, the mean length, and the setting for all blades are given in table II.

TABLE II.—COMPRESSOR BLADE DATA

Location	Number of blades	Chord (in.)	Approximate mean length (in.)	Blade angle ¹ (deg)	
				At hub	At casing
Entrance guide vanes	35	2.000	3 $\frac{1}{4}$	27	27.0
First rotor	22	1.350	2 $\frac{3}{4}$	40	70.8
First stator	25	1.350	2 $\frac{7}{8}$	42	56.0
Second rotor	26	1.350	2 $\frac{3}{4}$	41	54.7
Second stator	27	1.350	11 $\frac{5}{16}$	42	53.1
Third rotor	28	1.350	11 $\frac{1}{16}$	40	50.5
Third stator	29	1.350	1 $\frac{1}{2}$	41	49.6
Fourth rotor	30	1.350	1 $\frac{3}{4}$	39	47.2
Fourth stator	42	1.013	1 $\frac{9}{32}$	39	45.6
Fifth rotor	43	1.013	1 $\frac{1}{16}$	39	45.6
Fifth stator	44	1.013	1 $\frac{5}{16}$	40	45.4
Sixth rotor	45	1.013	1 $\frac{3}{16}$	39	44.1
Sixth stator	44	1.013	$\frac{3}{4}$	38	42.3
Seventh rotor	45	1.013	2 $\frac{1}{32}$	38	42.1
Seventh stator	46	1.013	1 $\frac{9}{32}$	36	39.4
Eighth rotor	47	1.013	1 $\frac{7}{32}$	36	² 39.3
Eighth stator	48	1.013	1 $\frac{7}{32}$	36	39.0

¹ All blade angles represent the angle between the tangent to the concave surface of the blade and the axis of the compressor. In the original tests the blade angle was measured at the base of the blade; in the final tests the blade angle was measured at the tip of blades because this method was more accurate.

² Owing to an error in setting, the blade angle for the eighth rotor row in the final tests was 2° greater than shown.

THEORY OF OPERATION

The purpose of the entrance guide vanes is to reduce the velocity relative to the first row of rotor blades and to approach symmetry of velocity diagrams in the rotor and the stator blades. This purpose is accomplished by imparting

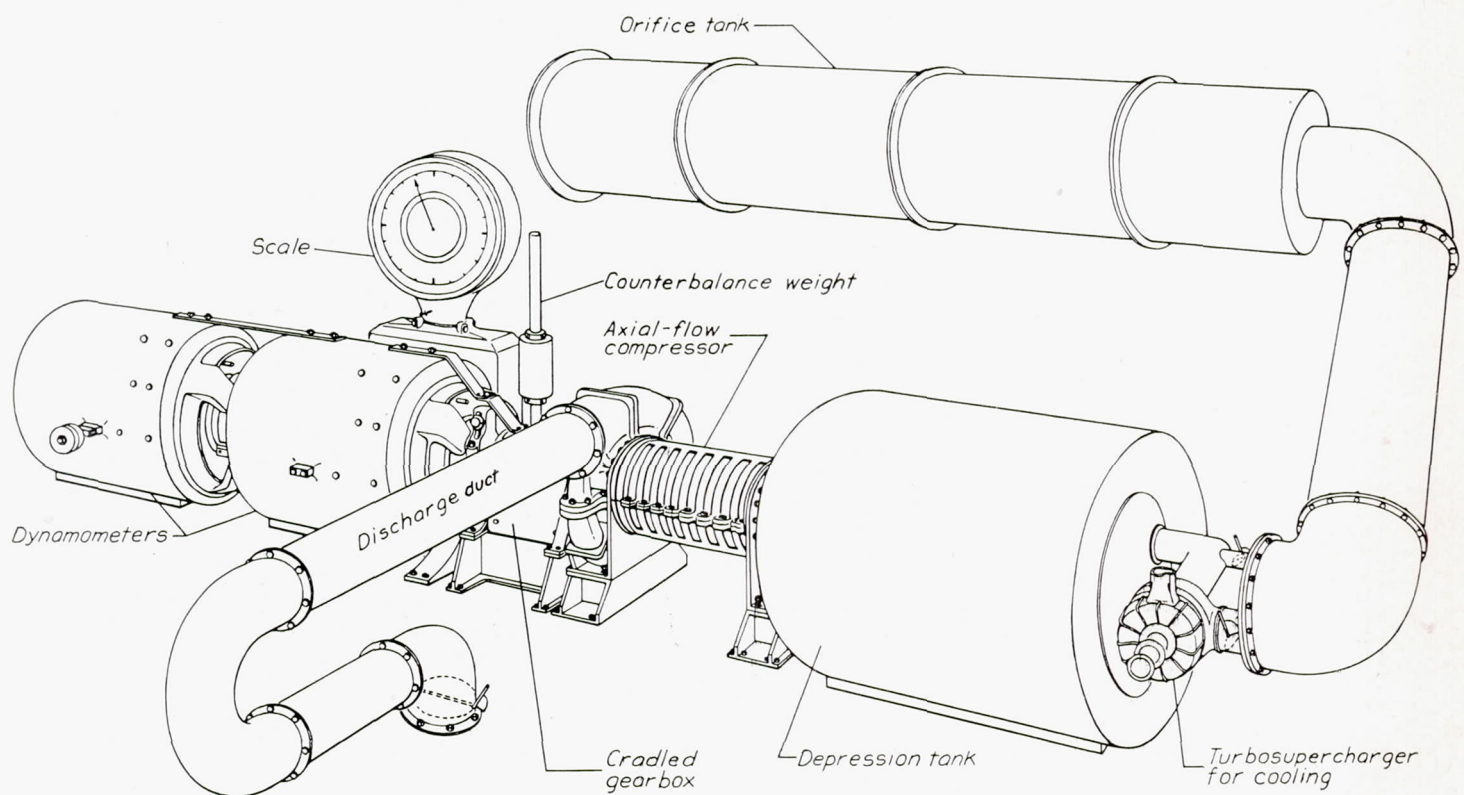


FIGURE 4.—Setup of equipment for tests of axial-flow compressor.

prerotation to the air entering the first rotor row; this prerotation, incidentally, causes a drop in static pressure due to the increase in velocity. The first rotor row imparts additional rotation to the air; work is done on the air and the total pressure is increased. The static pressure is also increased because the velocity relative to the rotor is decreased. The following stator row reduces the whirl velocity, which results in a further increase in static pressure. Throughout the compressor, the process is repeated: the rotor row increasing the absolute whirl velocity and the stator row decreasing it.

This process is essentially the same in the rotor and the stator blades; each row of blades acts as a row of diffusers decreasing the velocity relative to that row of blades and thereby increasing the pressure. Because of this similarity of function of the rotor and the stator blades, the condition for optimum performance should be essentially the same for each; that is, for optimum stage performance, the velocity diagrams for the rotor row and the stator row should be equivalent. This equivalence is attained by the use of a symmetrical velocity diagram for a given stage in which the velocity diagram for the rotor row is the mirror image of that for the stator row, and the mean whirl velocity is equal to half the rotor-blade velocity.

Because of the effects of centrifugal and Coriolis forces, true equivalence in the rotor and stator blades is impossible. In the rotor blades, the pressure rise across the blades must be greater at the casing than at the hub in order to balance the greater centrifugal force caused by the increase in whirl velocity following the rotor row; whereas, in the stator row, the reverse is true. The deviation from equivalence of the

diagram at each radius and an axial component of velocity that is constant with respect to the radius but increases along the axis from the inlet to the outlet end of the compressor. The increase in the axial component of velocity, used to obtain maximum pressure ratio per stage within the Mach number limitations imposed at the blade tips, is obtained by tapering the rotor. The design theory, based on an unpublished report by Eugene W. Wasielewski, is developed in the appendix.

APPARATUS AND TEST PROCEDURE

TESTS

The current standard procedure for testing superchargers was used as far as practicable. The setup of the test equipment is shown in figure 4. Because of necessary changes made in the setup during the tests, the results reported are for two sets of conditions which, for convenience, have been designated original and final tests and are given for easy reference in table III.

Original tests.—The compressor was driven by a 300-horsepower dynamometer interconnected with a cradled gearbox in order that the torque output might be read from a single scale. An adjustable counterbalance weight was mounted on the gearbox to obtain a center of gravity for the gearbox that would coincide with the compressor axis. The inlet air passed from an orifice tank through a valve into a depression tank approximately 4 feet in diameter and 6 feet in length. This depression tank had a felt filter and honeycomb straightening vanes to insure a smooth air flow free from foreign particles. Because of the large cross-sectional area of the tank, the velocity pressure was negli-

TABLE III.—SUMMARY OF CONDITIONS FOR ORIGINAL AND FINAL TESTS

Condition	Original tests				Final tests		
Bearings	Ball and roller				Journal and fixed-wedge thrust		
Dynamometer	1				2		
Blades set	At hub				At tip		
Inlet air	Room temperature		Cooled with small turbine		Varying degrees of cooling with larger turbine		
Type of test	Over-all performance		Over-all performance		Over-all performance	Speed parameter	Heat transfer
Lagging on compressor	None		None		None	None	1-inch felt
Speed	Rotor (rpm)	Blade tip (ft/sec)	Rotor (rpm)	Blade tip (ft/sec)	Rotor (rpm)	Blade tip (ft/sec)	Both the speed-parameter and heat-transfer tests were made at a rotor speed of approximately 11,000 rpm or a blade-tip speed of approximately 672 feet per second.
	5000	305.4	9,000	549.8	8,000	488.7	
	6000	366.5	10,000	610.9	10,000	610.9	
	7000	427.6	11,000	672.0	12,000	733.0	
	8000	488.7			13,000	794.1	
	9000	549.8			14,000	855.2	

rotor and the stator blades increases as the ratio of hub to casing diameter decreases. In the design of the NACA axial-flow compressor, only the pressure balance across a complete stage was considered (except for the initial guide vanes and first rotor row) and not across individual rows of blades. Some deviations from the design flow must therefore be expected.

The entrance guide vanes and the first row of rotor blades were designed to produce a whirl-velocity distribution approximately corresponding to a symmetrical velocity diagram at each radius. The following rows of blades and the passage shape were designed on the basis of a symmetrical velocity

gible. The discharge air from the compressor passed through a lagged discharge duct 8 inches in diameter and 10 diameters in length. The use of a depression tank at the compressor inlet instead of a straight duct 15 diameters in length, and a discharge duct of 10 diameters in length instead of 15 are the only changes from standard test procedure. The effect of these changes on the results is believed to be negligible. Tests made with this setup covered a range of rotor speeds from 5000 to 9000 rpm and a range of air flows from wide-open throttle to near surge. Because the compressor had a violent surge, no data were taken in the surge range.

At 9000 rpm, the discharge temperatures were becoming too high for the aluminum blades and the damaged bearings had to be replaced. In order to reduce the temperature throughout the compressor, the inlet air was cooled by expanding it through the turbine of a turbosupercharger; the supercharger served as a brake to regulate the speed of the turbine. Because the flow range of the turbine was limited, an inlet valve was used to obtain low air flows and a bypass valve was used to obtain high flows. The depression tank was lagged to reduce heat transfer to the cooled inlet air. Tests made with this setup covered a range of rotor speeds from 9000 to 11,000 rpm; at 11,000 rpm the ball and roller bearings failed.

Final tests.—The ball and roller bearings were replaced by the special journal and thrust bearings, a larger turbo-supercharger was installed, four thermocouples were placed symmetrically around the compressor inlet to check the

INSTRUMENTATION

Locations of the various measuring stations are shown in figure 5. The air temperature at the orifice-tank inlet was measured with mercury-in-glass thermometers; all other temperatures were measured with thermocouples. The air and oil temperatures were measured with copper-constantan thermocouples. The four thermocouples at the compressor inlet were symmetrically placed around the compressor axis; the two thermocouples after the last row of stator blades and the two thermocouples in the discharge duct were arranged diametrically opposite. The cold junctions of all thermocouples were placed in an ice bath to insure a constant temperature at the cold junction equal to that at which the thermocouples were calibrated. The difference in potential between the hot and the cold junction was measured with a calibrated potentiometer.

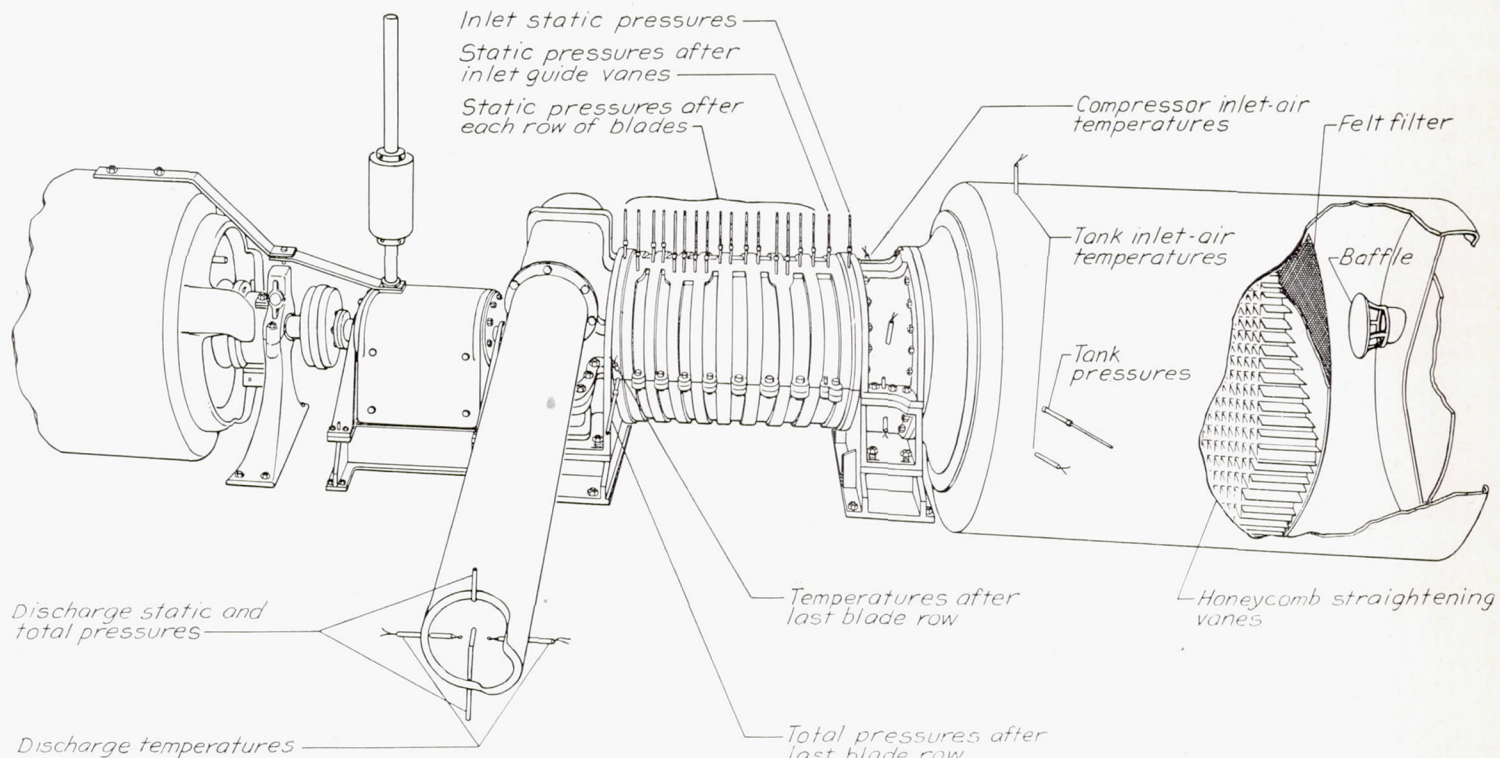


FIGURE 5.—Compressor setup showing location of pressure and temperature measuring stations.

tank thermocouples, the blades were reset by measuring the angles at the tip, and another 300-horsepower dynamometer was added to obtain more power. Performance tests were made over a range of speeds from 8000 to 14,000 rpm with the compressor and the scroll unlagged. Special speed-parameter tests were also made at 11,000 rpm with the compressor unlagged. In order to check adiabatic temperature-rise efficiency against adiabatic shaft efficiencies, the compressor and the scroll were lagged with felt 1 inch thick. Thermocouples and oil-weighing equipment were installed to measure the heat carried off by the oil. Special speed-parameter and heat-transfer tests were being made when the compressor blades failed at 11,000 rpm.

All static and total pressures, except the pressure drop across the thin-plate orifice, were measured with mercury manometers. Only static pressures were measured in the depression tank because the velocity pressure was negligible. Static pressures were taken at the compressor inlet, after the entrance guide vanes, and after each row of blades. Two total-pressure tubes were placed at the exit of the last row of blades to determine compressor efficiency without scroll losses.

The weight of air entering the compressor was determined with a thin-plate orifice. The pressure drop across the orifice was measured in millimeters of alcohol with an NACA micromanometer.

The desired constant speed was maintained with a speed strip and a stroboscopic tachometer operated on 60-cycle current. An electric tachometer was used only as a convenience in setting the speed at approximately the desired value. The speed was frequently checked with a counter and stop watch. The power input to the compressor was determined from torque measurements on a calibrated scale. The weight of oil flowing and the temperature rise of the oil were measured for each bearing in order to obtain the heat loss to the oil for the determination of the energy balance of the compressor.

PRECISION

Two possible sources of error may have appreciably affected the final results. When inlet-air cooling was used, a large temperature gradient was obtained across the depression tank in which the turbine-exit air and the bypass air were inadequately mixed. Because the arithmetical average of the inlet temperatures was used, the true flow average was probably not obtained. Calculations based on the highest and the lowest inlet-temperature readings indicate that the adiabatic temperature-rise efficiency could be in error as much as 3 percent. After the compressor-blade failure, a leak was discovered in the turbine inlet, which may have reduced the adiabatic shaft efficiency and the weight flows as much as 3 percent.

The accuracy of all measurements is estimated to be within the following limits:

Temperatures, °F	± 0.5
Pressures, inches of mercury	± 0.02
Compressor speeds, percent	± 0.5
Air-weight flows, percent	± 0.5
Torque-scale readings, percent	± 2

SYMBOLS

<i>a</i>	local velocity of sound, feet per second
<i>B</i>	number of blades in row
<i>c</i>	blade chord, feet
<i>c_p</i>	specific heat at constant pressure
<i>c_v</i>	specific heat at constant volume
<i>C_L</i>	lift coefficient based on mean relative velocity
<i>D</i>	drag per unit blade length, pounds per foot
<i>D_t</i>	rotor-blade tip diameter, feet
<i>F</i>	resultant force on blades per unit blade length, pounds per foot
<i>g</i>	standard acceleration of gravity, 32.174 feet per second per second
<i>H_{ad}</i>	isentropic increase in total enthalpy per unit mass for given total-pressure ratio, foot-pounds per pound
<i>L</i>	lift per unit blade length, pounds per foot
<i>M</i>	local Mach number, V/a
<i>M_c</i>	compressor Mach number, U_t/a_1
<i>n</i>	rotor speed, rps
<i>p</i>	absolute pressure, pounds per square foot
<i>P</i>	power per unit blade length, foot-pounds per second per foot
<i>q_{ad}</i>	pressure coefficient, gH_{ad}/U_t^2
<i>Q</i>	volume rate of flow, cubic feet per second
<i>Q_{1/n}</i>	load coefficient

Q_1/nD_t^3	quantity coefficient
<i>r</i>	radius to blade element, feet
<i>S</i>	blade spacing, $2\pi r/B$, feet
<i>T</i>	total temperature, °R
<i>u</i>	ratio of rotor-blade-element velocity to axial component of air velocity, U/V_a
<i>U</i>	velocity of rotor-blade element ($2\pi rn$) at radius <i>r</i> , feet per second
<i>V</i>	air velocity, feet per second
<i>w</i>	ratio of relative whirl component of air velocity to axial component
Δw	ratio of increase in relative whirl component across blade row to axial component of air velocity (normally negative)
β	angle between compressor axis and air velocity, degrees
γ	adiabatic exponent, c_p/c_v
Γ	circulation around blade, square feet per second
ζ	loss ratio, $P_{L,T}/P_I$
η	blade-element efficiency for stage
η_T	adiabatic temperature-rise efficiency
η_s	adiabatic shaft efficiency
θ	ratio of inlet-air total temperature to NACA standard sea-level temperature (518.6°R)
ρ	mass density of air, slugs per cubic foot
σ	blade-element solidity, $cB/2\pi r$

SUBSCRIPTS:

1	conditions at compressor inlet (1a, 1b, 1c in depression tank; 1d, 1e, 1f, 1g just ahead of entrance guide vanes)
2	conditions just after last row of stator blades
3	conditions in discharge duct from compressor
<i>a</i>	axial component
<i>c</i>	compressor
<i>h</i>	at hub
<i>id</i>	ideal
<i>I</i>	input
<i>L</i>	loss (except C_L)
<i>m</i>	relative to mean of inlet and exit velocities for row of blades
<i>R</i>	rotor
<i>S</i>	stator
<i>s</i>	static (except η_s)
<i>t</i>	at rotor blade tip or casing
<i>T</i>	total (except η_T)
<i>u</i>	useful
θ	tangential direction

RESULTS AND DISCUSSION

All of the performance tests of the axial-flow compressor except a few special speed-parameter and heat-transfer tests were made with rotor speed as the parameter, in accord with general supercharger practice of 1940. The performance curves plotted on that basis, however, are accurate only for the particular inlet-air temperature used in the tests. The performance data were later replotted on a nondimensional basis to permit evaluation of performance at any desired temperature.

Tests of the compressor were made at speeds from 5000 to 14,000 rpm at increments of 1000 rpm. The adiabatic temperature-rise efficiency of the compressor increased from 66 percent at 5000 rpm to 87 percent at 14,000 rpm, an average increase of more than 2 points for each 1000-rpm increase in speed (fig. 6). At an inlet-air temperature of 45° F and an inlet volume flow of 129.3 cubic feet per second, which results in a compressor Mach number of 0.77, a peak adiabatic temperature-rise efficiency of 87 percent and an over-all pressure ratio of 3.42 were obtained, showing that high-efficiency multistage axial-flow compressors can be designed by the application of airfoil theory.

PERFORMANCE TESTS WITH ROTOR SPEED AS PARAMETER

Because the original tests were at low speeds and the final tests were at high speeds with an overlapping range, the effect of changes in test conditions on performance can be determined from the overlapping range.

Comparison of original and final tests.—The difference in performance between the original and the final tests is shown in figure 6. This difference may have been caused by changes in blade setting, cooling of the inlet air, or bearings. (See table III.) The original tests were made at speeds from

5000 to 11,000 rpm and the final tests from 8000 to 14,000 rpm, with a resultant overlapping range from 8000 to 11,000 rpm. This overlapping range, which makes possible the comparison of the low-speed and the high-speed tests, shows that the effect of changes in test conditions was small. The blade setting in the final tests gave a slight increase in efficiency but gave a smaller air flow than the original blade setting, as shown by the tests at 10,000 and 11,000 rpm. The blade setting plus the effect of cooling in the final tests gave a greater increase in efficiency than did blade setting alone, as indicated by the tests at 8000 rpm. At 8000 rpm also, the effect of cooling on flow counteracted the effect of blade setting with the result that the volume flow was the same for both the original and the final tests. The different bearings in the original and final tests may have had a slight effect on adiabatic temperature-rise efficiency because in the original tests, the heat generated in the front roller bearing was transferred to the compressor air, whereas in the final tests, part of the heat generated in the front journal bearing was carried off by the lubricating oil. Calculations indicated that changing the rear bearings should have a negligible effect on the compressor performance because of the long heat-transfer path involved. Because this difference between

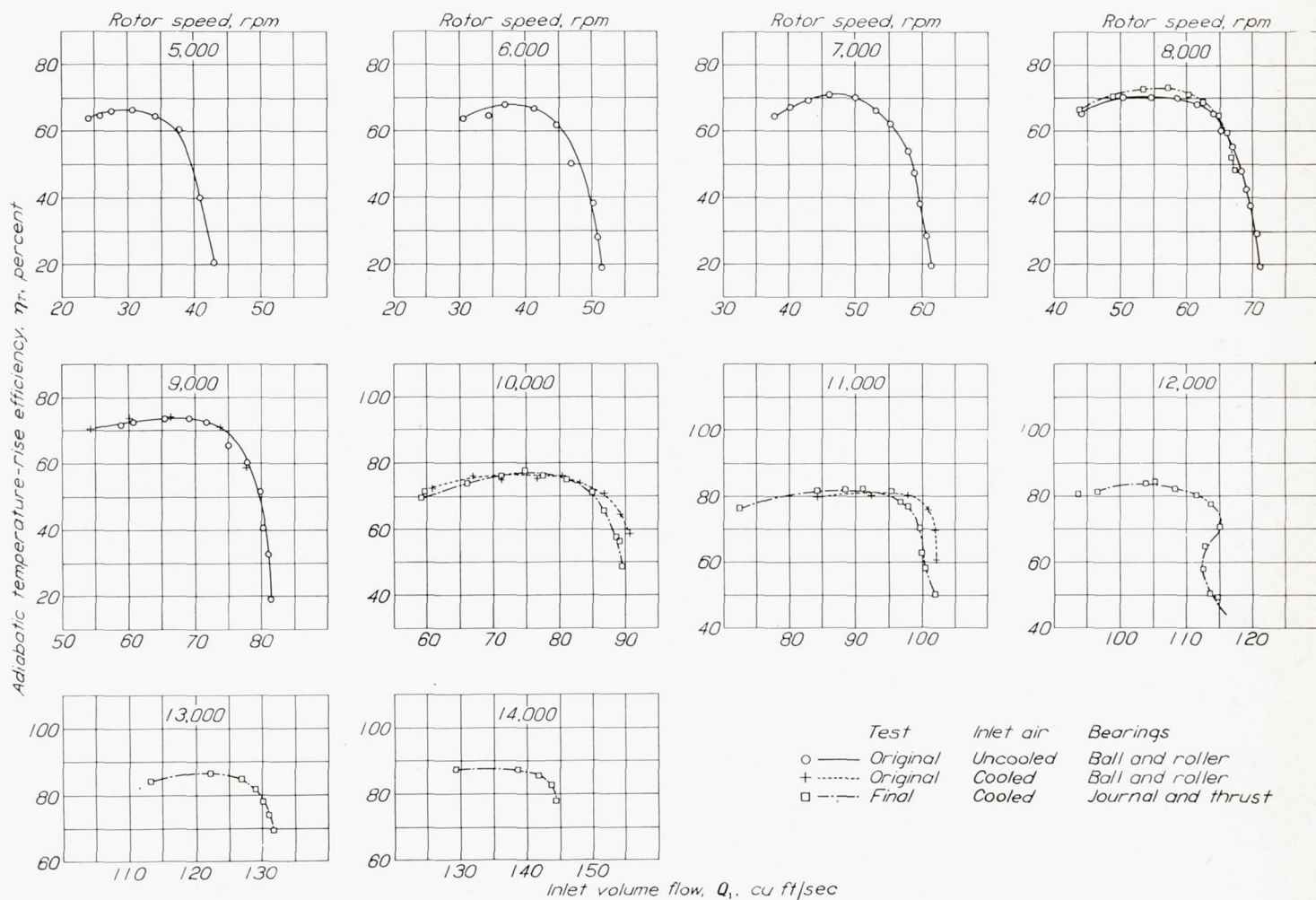


FIGURE 6.—Effect of volume flow and rotor speed on adiabatic temperature rise efficiency. Compressor unlagged.

the original and the final results is so small as to be almost within the experimental error, the tests at low speeds can be compared with those at high speeds with a fair degree of accuracy.

Performance at different rotor speeds.—Inasmuch as the compressor was designed on a Mach number basis, the design rotor speed depends upon the inlet-air temperature; that is, the design speed is 16,000 rpm at -67° F, and 18,400 rpm at 59° F. Because of the large efficiency variation with speed, the choice of a parameter to represent the speed is especially important. Dimensional analysis shows that compressor performance does not depend upon rotor speed alone but is a function of dimensionless variables, such as the compressor Mach number U_t/a_1 where U_t is the rotor blade-tip velocity and a_1 is the velocity of sound at the inlet to the compressor.

In figure 7 the peak adiabatic temperature-rise efficiency is plotted as a function of the compressor Mach number. Because of the slight differences in blade settings, separate curves are drawn through the points obtained in the original and the final tests. The points in the final tests fit the straight line quite well, but those of the original tests show an appreciable scatter from the linear relation. The final high-speed tests have slightly higher efficiency than the original low-speed tests in the overlapping range (fig. 6); this difference appears to increase with speed and may amount to 4 points at maximum test speed. (See fig. 7.) The linear relation cannot, of course, hold at high values of U_t/a_1 owing to compression shock losses encountered when the relative air velocity at any point exceeds the local velocity of sound. Because the local Mach number is a function of the compressor Mach number and the load coefficient Q_1/n , the peak efficiency must reach a maximum at a value of U_t/a_1 probably greater than values herein reported. A leveling-off of the efficiency curve at the highest volume flow is indicated in figure 7 but, because of the limited number of test points at 14,000 rpm, definite conclusions are unwarranted.

The increase in efficiency with speed was expected because the flow distribution approaches the design distribution as

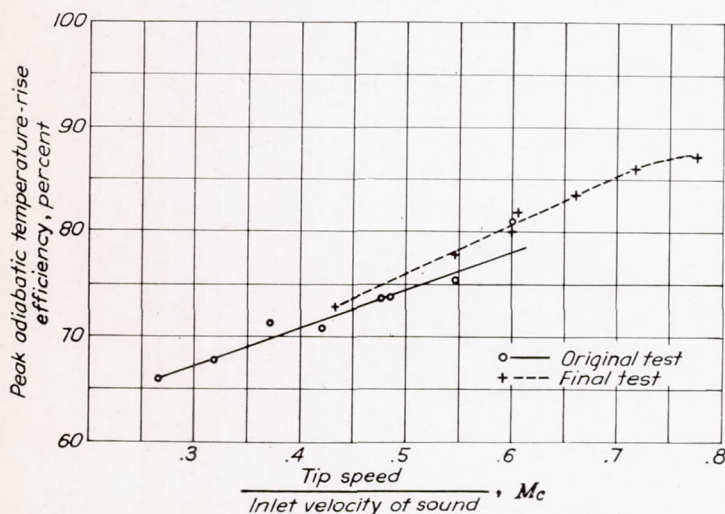


FIGURE 7.—Relationship between peak adiabatic temperature-rise efficiency and ratio of tip speed to inlet velocity of sound. Compressor unlagged.

the speed increases. At low rotor speeds when the axial component of velocity is correct at the middle of the compressor, the velocity will be too low at the inlet with resultant high angles of attack accompanied by large losses and will be too high at the outlet with resultant small angles of attack and too little work from the last rotor blades. Losses in the scroll will also be high because of the high outlet velocity. Efficiencies at low speeds could have been improved by using different blade settings for each speed, but such investigations would have required considerable time. Because the tests were planned for performance at design conditions, the blade settings were not altered to give maximum performance at different speeds but were set for the design speed throughout the tests.

Compressor efficiencies based on total-pressure measurements at exit of last stator row.—In order to investigate compressor efficiencies without including losses in the scroll collector, provision was made for taking total-pressure surveys behind the last row of stator blades. Because of the urgency for data on over-all performance, these surveys were to be made after the regular performance tests had been completed; owing to blade failure, these surveys were never carried out. In the course of taking other data, however, readings were taken on two total-pressure tubes adjusted in the center of the stream to give maximum-pressure readings. The adiabatic efficiencies based on the average of these two readings are shown in figure 8; the over-all efficiencies of the compressor-scroll combination are shown for comparison. Compressor efficiencies based on these two total-pressure readings will be somewhat higher than efficiencies based on passage surveys; the difference will vary with Q_1 , owing to variation in velocity pressure and velocity distribution. The results must therefore be considered approximate.

The greatly increased spread between the over-all efficiency of the compressor-scroll combination and the efficiency of the compressor proper at the higher values of Q_1 is caused by the large increase in kinetic energy of the air entering the scroll. Because the static-pressure ratio across the compressor proper (static pressure at 8s divided by tank pressure) drops considerably with a small increase in Q_1 (see fig. 9), the outlet velocity must increase much more rapidly than Q_1 , which results in a large increase in scroll losses for a small increase in Q_1 . The outlet velocity may approach the velocity of sound at the higher compressor speeds with wide-open throttle. The local Mach number at the compressor outlet can be calculated from the formula

$$M = \frac{V}{a} = \sqrt{\frac{2}{\gamma-1} \left[\left(\frac{p_T}{p_s} \right)^{\frac{\gamma-1}{\gamma}} - 1 \right]}$$

The total and the static pressures can be obtained from the curves of figure 9 at location 8s.

The sudden drop in efficiency at wide-open throttle with a Q_1 of 114.6 cubic feet per second and at a rotor speed of 12,000 rpm can be explained by compression shock losses over the last stator blades; the Mach number following these blades was 0.938. The sudden drop in efficiency

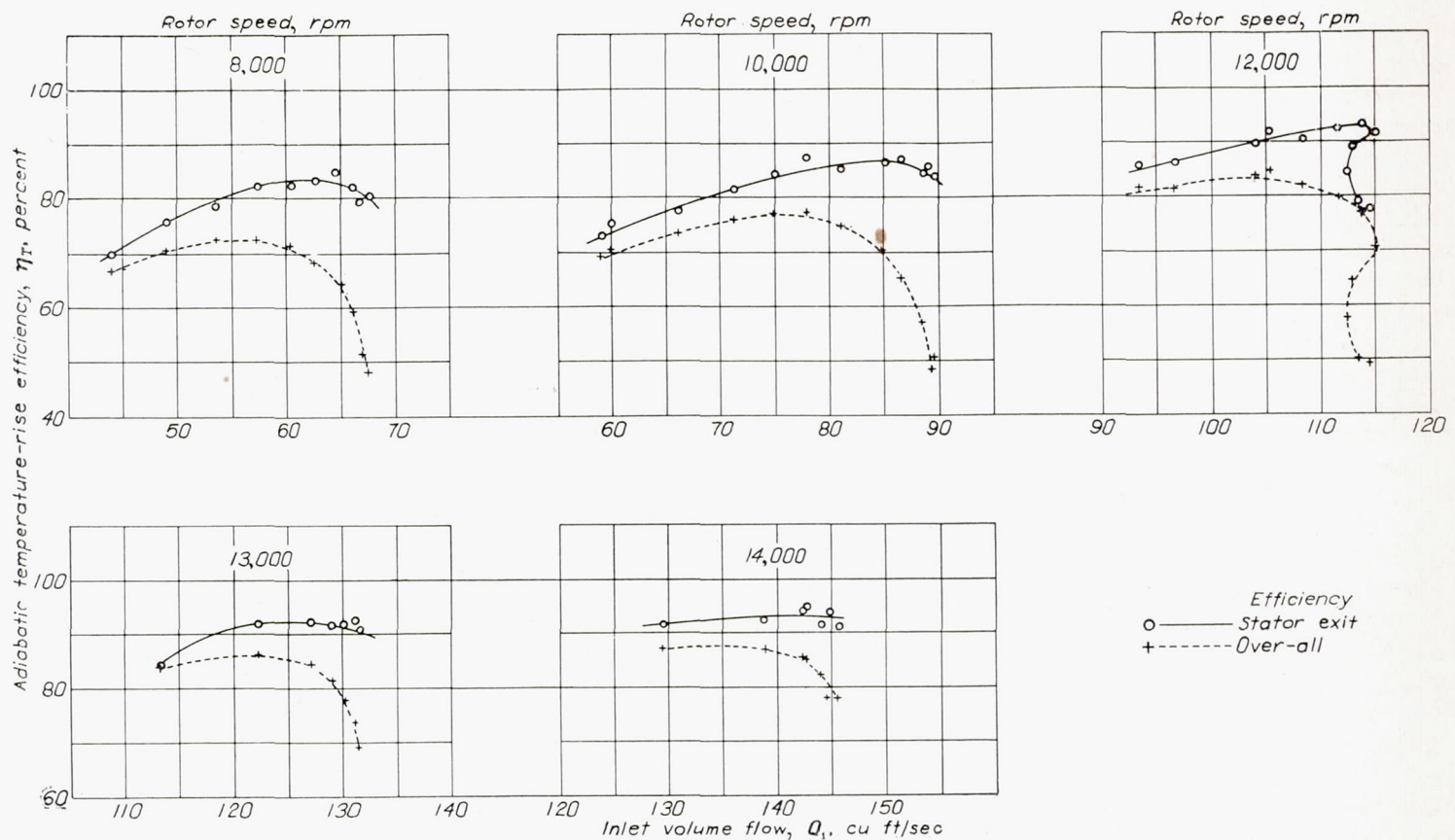


FIGURE 8.—Comparison of over-all efficiency with efficiency based on total-pressure measurements after last row of stator blades at varying speed and volume flow. Compressor unlagged.

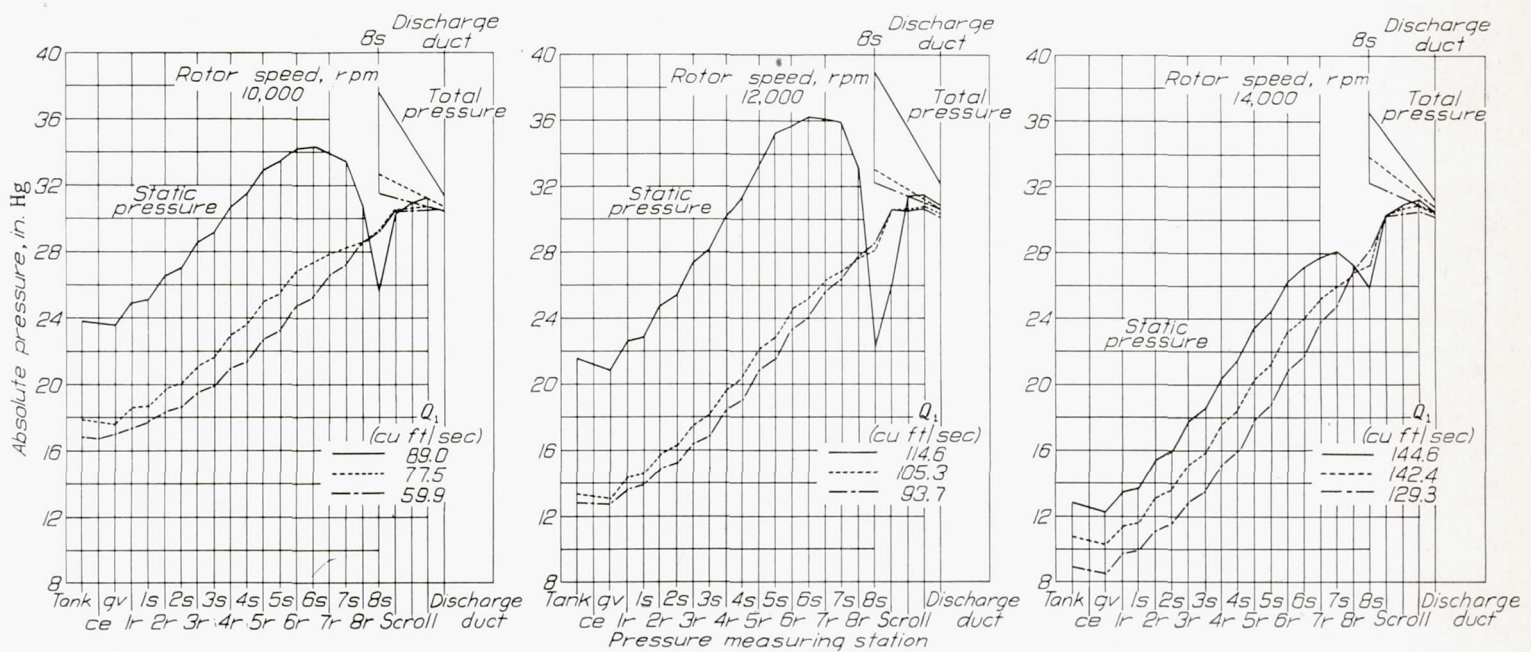


FIGURE 9.—Pressure variation from inlet tank to discharge duct for varying speed and volume flow: at compressor entrance ce; after guide vanes gv; after each row of rotor blades 1r . . . 8r; after each row of stator blades 1s . . . 8s. Compressor unlagged.

with increase in Q_1 did not occur at other speeds because the exit velocities were well below sonic values. At lower compressor speeds, losses were sufficient even at wide-open throttle to keep velocities well below sonic values; because of power limitations, tests at higher speeds were not run at wide-open throttle where sonic velocities would be encountered.

Pressure distribution through the compressor.—The pressure distribution through the compressor is shown in figure 9. In addition to the static pressures, total pressures taken at the exit of the last stator blades (location 8s) and in the discharge duct are shown.

The pressure rise toward the outlet end of the compressor is markedly sensitive to changes in Q_1 , actually becoming negative for large values of Q_1 . The much larger change in pressure rise at the discharge than at the inlet is caused by compressibility effects. A small increase in Q_1 produces a

small increase in the axial component of velocity at the inlet and a decrease in the angle of attack. The smaller angle of attack results in a smaller density ratio and, because of continuity, produces a somewhat greater increase in the axial component of velocity behind the row of blades than ahead of the row. The effect may be quite small in the first few rows of blades and actually masked by other effects, such as a change in velocity distribution in the radial direction, but the cumulative effect over a number of stages may become so large that in the last stage negative angles of attack result on both rotor and stator blades. The last stage then acts as a turbine recovering part of the energy put in by the preceding stages.

CORRELATION OF VARYING INLET-AIR-TEMPERATURE DATA BY USE OF DIFFERENT SPEED PARAMETERS

The large variation of adiabatic efficiency with compressor speed, the wide range of inlet-air temperatures used, and

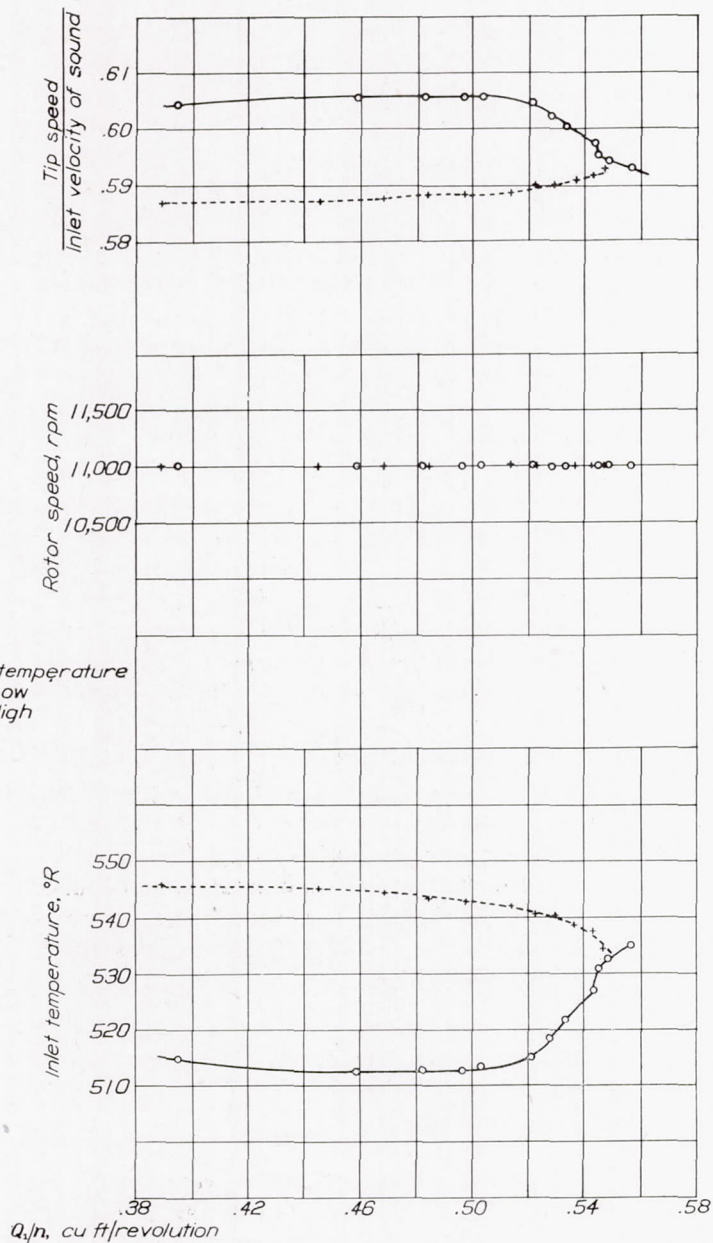
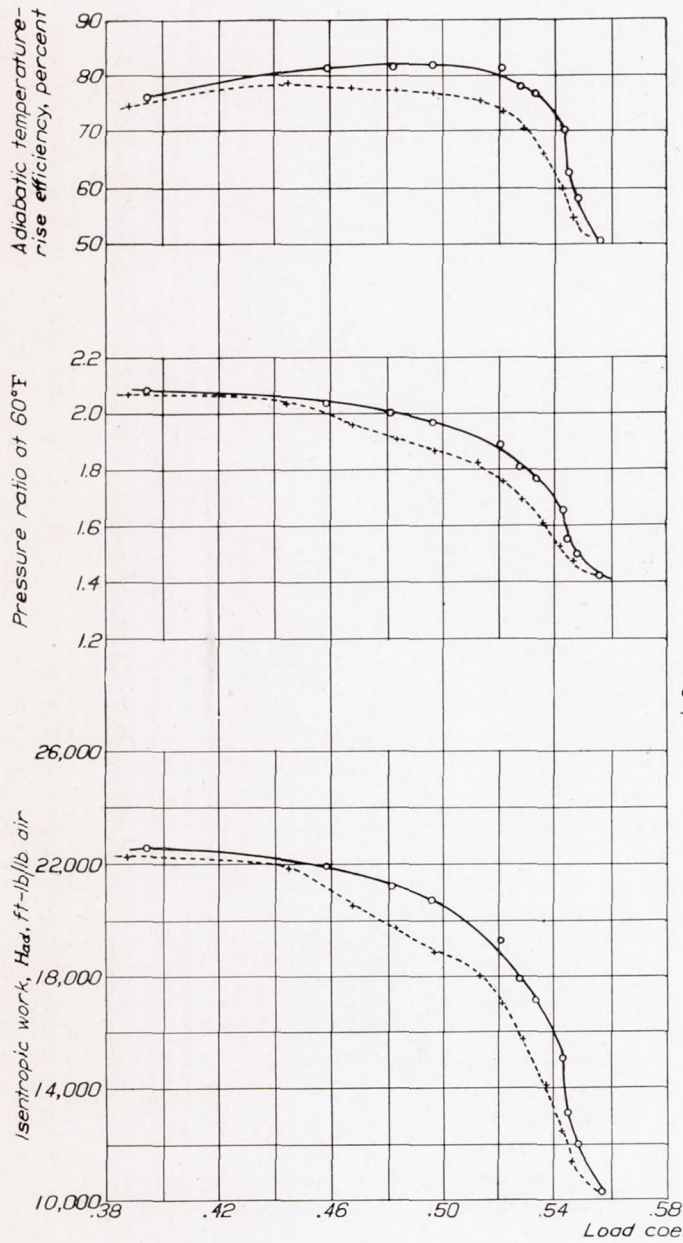


FIGURE 10.—Effect of inlet air temperature on performance characteristics at constant rotor speed of 11,000 rpm. Compressor unlagged.

certain peculiarities of the performance curves when rotor speed was used as a parameter (note shape of curve for 12,000 rpm at high volume flow, figs. 6 and 8) made the investigation of the effect of inlet-air temperature with different speed parameters imperative.

Constant rotor speed.—Tests were run at a constant rotor speed of 11,000 rpm and at two sets of inlet-air temperatures to investigate the effect of inlet-air temperature on the shape of performance curves. Starting with the turbine-inlet and the bypass throttles wide open, the maximum amount of cooling for the desired range of flows was obtained by first closing the bypass throttle and then closing the turbine-inlet throttle until the surge point was reached. The tests were repeated to obtain the maximum temperature by first closing the turbine-inlet throttle and then the bypass throttle.

The results of these tests are shown in figure 10. The marked difference between the two sets of curves indicates that the compressor performance based on rotor speed as a parameter depends to an appreciable extent on the inlet-air temperature. Although the temperature could be considered an additional variable, in representing results the number of independent variables should be kept as small as possible. Dimensional analysis is of value in determining the minimum number of independent variables once the essential factors of the problem are known. (For a discussion of the methods of dimensional analysis as applied to air compressors see reference 35.)

Constant ratio of tip speed to velocity of sound.—If the effect of viscosity, heat transfer, deformation of compressor, and variation of specific heat are neglected, dimensional analysis shows that the performance of any set of geometrically similar compressors should depend on two dimensionless variables, which may be taken as Q_1/nD_t^3 and U_t/a , where D_t is the diameter of the rotor blade tip and a is either the velocity of sound at the inlet a_1 or at the discharge a_3 . When only one compressor is considered, D_t may be omitted because it remains constant. The quantity coefficient Q_1/nD_t^3 is thus replaced by the load coefficient Q_1/n .

In order to determine whether two independent variables are sufficient for representing the performance of the axial-flow compressor, the tests with two sets of inlet-air temperatures were repeated, first with U_t/a_1 and later with U_t/a_3 held constant. The results are shown in figure 11. Check runs were made for both high and low inlet temperatures with U_t/a_1 constant; these runs explain the two sets of high- and low-temperature curves in figure 11 (a). The quantities plotted in figure 11 differ from those in figure 10 to conform to dimensional considerations; the actual pressure ratio replaces the pressure ratio corrected to 60° F, and the dimensionless pressure coefficient

$$q_{ad} = \frac{H_{ad}}{V^2/g}$$

replaces the dimensional quantity H_{ad} .

The effect of inlet-air temperature on compressor performance was much less than when the rotor speed was held constant. A slight difference in performance, however, still existed for the two sets of inlet-air temperatures even

when the compressor Mach number was held constant, indicating that factors other than those considered in the simplified analysis had an effect on the performance. The Reynolds number effect affords the most reasonable explanation of the difference; the higher Reynolds number gives the higher efficiency, which is in accord with test results on airfoils. The change of 2 points in the compressor efficiency for only a 25-percent change in Reynolds number may be attributed to a critical Reynolds number effect found to occur on airfoils at approximately the Reynolds number encountered in the compressor tests. (See reference 36.) Other possible explanations were considered but were found to be inadequate to account for the results. Direct heat-transfer effects should produce a change in the opposite direction. Water condensation was eliminated as an explanation because all the tests were run at temperatures above the dew point at the inlet to the compressor.

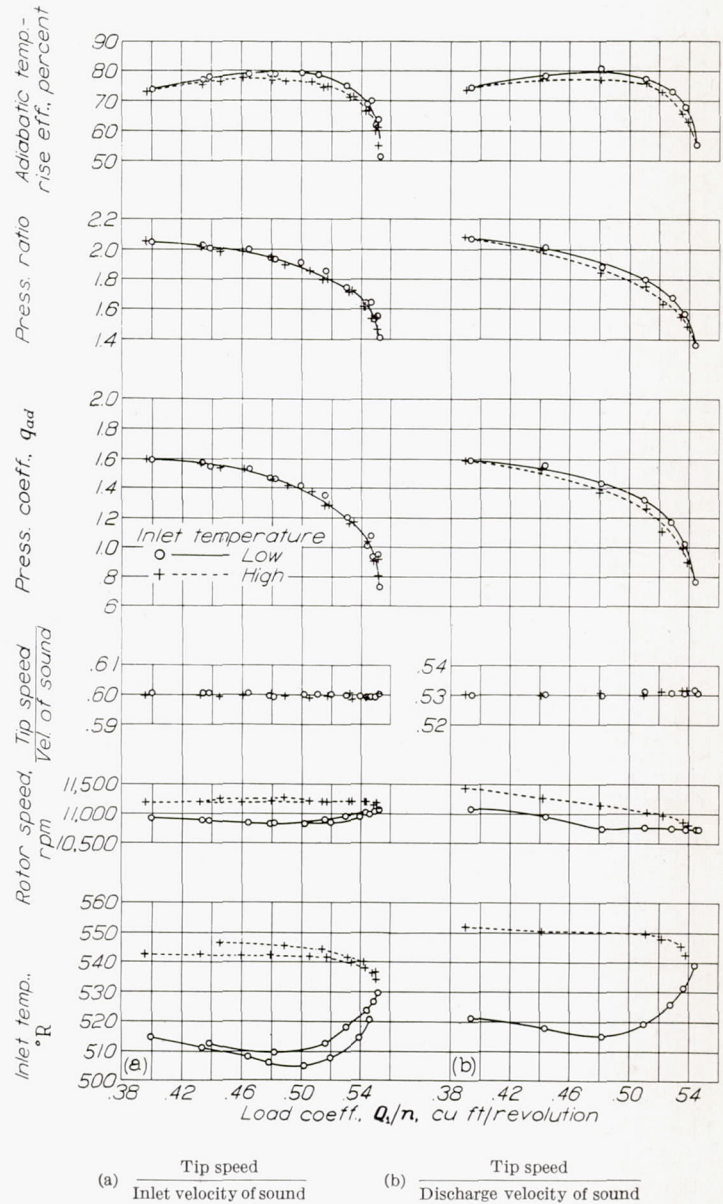


FIGURE 11.—Effect of inlet-air temperature on performance characteristics at constant ratio of tip speed to inlet and discharge velocity of sound. Compressor unlagged.

REPLOTTING OF ALL COMPRESSOR TESTS ON THE BASIS OF MACH NUMBER

Because the compressor Mach number was shown to offer a more accurate basis for performance representation than compressor speed, all the test results were replotted on the basis of Mach number (fig. 12). Instead of using the load

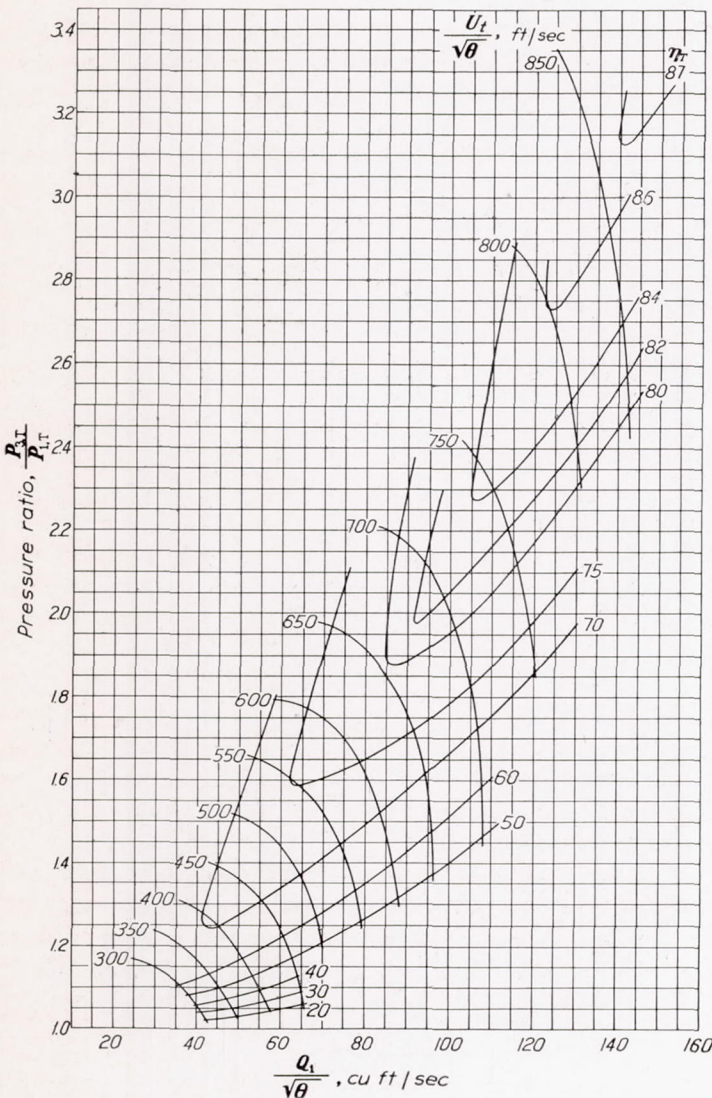


FIGURE 12.—Relationship of rotor speed, adiabatic temperature-rise efficiency, volume flow, and pressure ratio corrected to inlet-air temperature of 59° F. Compressor unlagged.

coefficient as abscissa and the compressor Mach number as a parameter (fig. 11), a method of representation proposed by Lt. Comdr. William Bollay in an unpublished report from the Bureau of Aeronautics, Navy Department, has been used. The total-pressure ratio is plotted as ordinate and $Q_i/\sqrt{\theta}$ as abscissa with $U_t/\sqrt{\theta}$ as a parameter, where θ is the temperature ratio $T_1/518.6$. As the over-all performance tests on the compressor were not run with $U_t/\sqrt{\theta}$ as a parameter, it was necessary to interpolate from test points to obtain both the $U_t/\sqrt{\theta}$ and the η_T contours.

The purpose of this method of representation is to give the performance directly in terms of the blade tip speed and the inlet volume flow at a standard inlet-air temperature of 59° F; the method at the same time permits ready calculation of the corresponding tip speed and inlet volume

flow at any other inlet-air temperature by multiplying the parameter $U_t/\sqrt{\theta}$ or the abscissa $Q_i/\sqrt{\theta}$, respectively, by the value of $\sqrt{\theta}$ for the desired temperature. The term $U_t/\sqrt{\theta}$ is, of course, directly proportional to the compressor Mach number. For reference, the values of the compressor Mach number corresponding to the values of $U_t/\sqrt{\theta}$ shown in figure 12 are given in the following table.

$U_t/\sqrt{\theta}$	U_t/a_1	$U_t/\sqrt{\theta}$	U_t/a_1	$U_t/\sqrt{\theta}$	U_t/a_1	$U_t/\sqrt{\theta}$	U_t/a_1
300	0.2688	450	0.4033	600	0.5377	750	0.6721
350	.3136	500	.4481	650	.5825	800	.7169
400	.3585	550	.4929	700	.6273	850	.7617

Although this representation includes the Mach number effect on performance, it does not include effects due to Reynolds number, heat transfer, etc., and therefore should not be expected to apply accurately to test conditions differing widely from those used in the performance tests.

HEAT TRANSFER AND SHAFT EFFICIENCIES

Although adiabatic efficiencies based on temperature-rise ratio are commonly used for rating superchargers, these efficiencies should, when possible, be checked against adiabatic shaft efficiencies based on measurements of power input and bearing losses. Adiabatic shaft efficiencies based on a shaft power defined as power input to compressor minus power loss in bearings should agree with the adiabatic efficiencies based on temperature-rise ratio, provided that the net heat loss from the compressor air is negligible.

Comparison of adiabatic temperature-rise, corrected shaft, and uncorrected shaft efficiencies.—Only a few runs had been made to compare the adiabatic temperature-rise and the shaft efficiencies corrected and uncorrected for bearing loss and to eliminate the sources of discrepancy when the test program was terminated by blade failure. Figure 13 presents results obtained at a compressor Mach number of

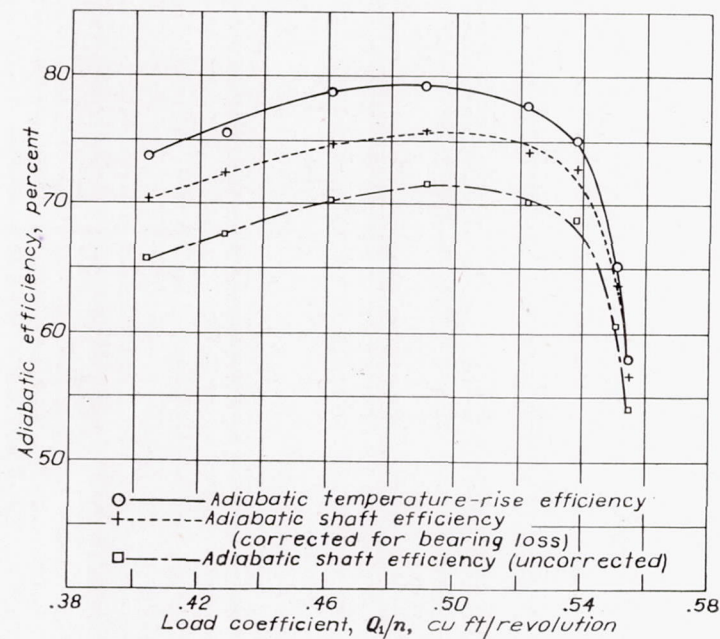


FIGURE 13.—Comparison of adiabatic temperature-rise efficiency with adiabatic shaft efficiency with and without correction for heat loss to oil. Ratio of tip speed to inlet velocity of sound, 0.6; compressor lagged.

0.6. The difference between the adiabatic temperature-rise efficiency and the corrected adiabatic shaft efficiency ranges from 1.3 to 4.2 points.

Figure 14 shows the variation of these efficiencies with time for constant rotor speed and air flow. The curves shown were based on the temperature measured by the four thermocouples at the compressor inlet and three thermocouples in the depression tank. The thermocouples at both locations were recalibrated after the compressor-blade failure and were found to be accurate. The difference between the curves based on the two sets of inlet-air temperatures was perhaps caused by failure to obtain a true flow-average temperature at either cross section because of the large variation in temperature across the section. Radiation from the hot rotor and the bearing supports may have affected the readings at the compressor inlet.

The data of figure 13 show a varying discrepancy between the adiabatic shaft efficiency and the adiabatic temperature-rise efficiency. The large differences in readings for the inlet thermocouples indicate an appreciable probable error for the inlet-air temperature, which was based on an arithmetical average. This error could make the adiabatic temperature-rise efficiency too high. A small leak discovered in the turbine after the completion of the tests, however, may have made the weight flow and the adiabatic shaft efficiencies too low. These sources of error probably account for the observed discrepancy.

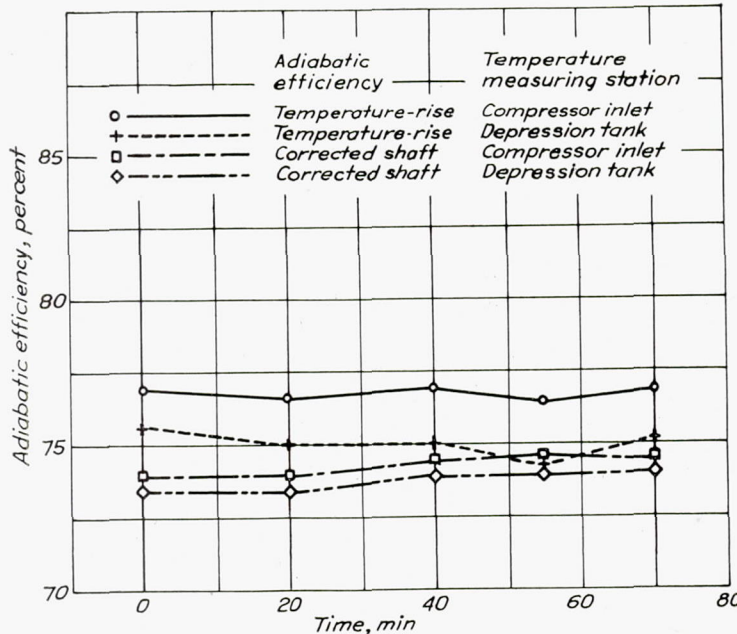


FIGURE 14.—Change in adiabatic temperature-rise efficiency and corrected adiabatic shaft efficiency during 70-minute stabilization test. Rotor speed, 11,000 rpm; volume flow, 89 cubic feet per second; compressor lagged.

Effect of lagging on adiabatic temperature-rise efficiency.—The effect of lagging on the adiabatic temperature-rise efficiency can be determined from the heat-transfer tests with the compressor lagged with 1-inch felt and the previous tests with the compressor unlagged. Figure 13 shows the adiabatic temperature-rise efficiency with lagging on the compressor at a compressor Mach number of 0.6. The peak adiabatic temperature-rise efficiency is reduced about 1 percent by lagging at this speed and would probably be reduced slightly more at higher compressor speeds.

SUMMARY OF RESULTS

Performance tests of the NACA axial-flow compressor at varying speeds gave the following results:

1. The adiabatic temperature-rise efficiency with the compressor unlagged increased with the compressor speed from a peak value of 66 percent at 5000 rpm to 87 percent at 14,000 rpm and was still increasing slightly with speed at 14,000 rpm.

2. A pressure ratio of 3.42 was obtained at a rotor speed of 14,000 rpm at the point of maximum efficiency. At this point the inlet volume flow was 129 cubic feet per second and the compressor Mach number was 0.776.

3. Tests at a rotor speed of approximately 11,000 rpm (compressor Mach number of 0.6) showed that lagging the entire compressor reduced the adiabatic temperature-rise efficiency by only about 1 point.

4. The adiabatic shaft efficiency corrected for heat losses to the lubricating oil and measured on the lagged compressor at a compressor Mach number of 0.6 was from 1 to 4 points lower than the adiabatic temperature-rise efficiency. Possible sources of error existed in both efficiency measurements.

5. Speed-parameter tests made over a range of inlet-air temperatures showed that the use of compressor Mach number as a parameter gave much better agreement of results at different temperatures than the conventional use of rotor speed as a parameter.

CONCLUSION

Axial-flow compressors of high efficiency can be designed by the proper application of airfoil theory.

AIRCRAFT ENGINE RESEARCH LABORATORY,
NATIONAL ADVISORY COMMITTEE FOR AERONAUTICS,
CLEVELAND, OHIO, August 1, 1944.

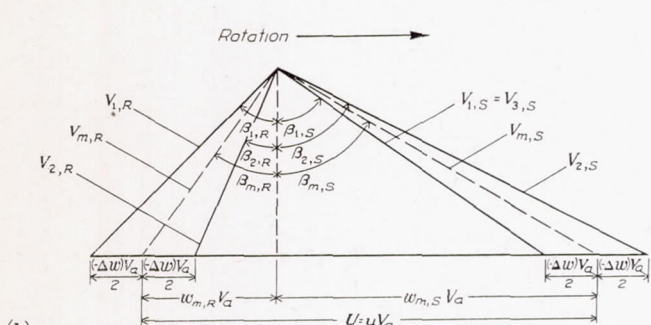
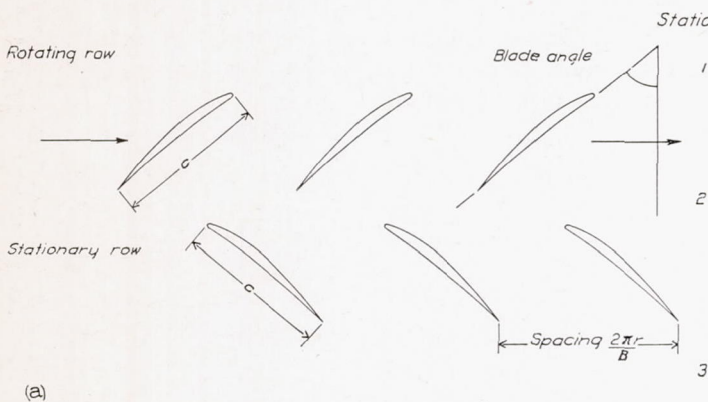
APPENDIX

DESIGN THEORY

EFFICIENCY OF RADIAL ELEMENT OF SINGLE STAGE OF COMPRESSOR

A typical stage of an axial-flow compressor consists of a row of rotating blades that increases the absolute whirl of the air and a row of stationary blades that decreases the absolute whirl. For the design theory of a single stage, the flow is assumed to be incompressible and to follow along cylindrical surfaces. Effects of radial flow components are therefore neglected. Shear forces along the cylindrical surfaces and circumferential variations in velocity and pressure are also neglected. On the basis of these assumptions, the flow in the annular space between the cylindrical surfaces at radii r and $r + dr$ may be considered as equivalent to the incompressible flow through an infinite two-dimensional cascade obtained by developing the cylindrical section at radius r . Figure 15 (a) shows the developed view at radius r of such a stage.

Figure 15 (b) shows the velocity diagram for the stage of figure 15 (a) with the corresponding stations indicated by the subscripts 1, 2, and 3. Quantities taken with the rotor blades as reference frame are indicated by the subscript R and with the stator blades as reference frame by the subscript S . When a single row of blades is being considered, a reference frame with respect to these blades is understood



(a) Development of cylindrical section of single stage.

(b) Velocity diagram for single stage.

FIGURE 15.—Velocity through cylindrical section of single stage of compressor.

and the subscripts R or S are omitted. The vector mean of the inlet and outlet velocities for a row of blades V_m (fig. 15 (b)) is for brevity referred to as the mean velocity. Certain velocity ratios used in the theory are defined as follows: u is the rotor-blade-element velocity divided by the axial component of air velocity; w , the relative whirl component of air velocity divided by the axial component; and $-\Delta w$, the decrease in relative whirl component of air velocity through the row of blades divided by the axial component.

In order to apply the principles of airfoil theory to a cascade of blades, it is necessary to generalize the concepts of lift and drag used for isolated airfoils. It can be shown (reference 16, pp. 4 and 5) that, for frictionless incompressible flow with constant axial velocity, the resultant force acting on a blade of a two-dimensional cascade is normal to the mean velocity V_m , and, per unit span, is given by

$$L = \rho V_m \Gamma$$

This equation is identical with the one given by the Kutta-Joukowski theorem for an isolated airfoil with the mean relative velocity V_m substituted for the free-stream velocity. Because of the close analogy to isolated airfoil theory, this force is called the lift. For viscous fluids, as in the case of isolated airfoils, there is also a component of force parallel to the mean velocity, which is called the drag. The resultant force is no longer normal to the mean velocity, but the component of the resultant force normal to the mean velocity is still called the lift although it will differ from the lift for frictionless flow with the same velocity diagram.

The aerodynamic forces, per unit blade length, acting on a blade element are shown in figure 16 in which L is the lift; D , the drag; F , the resultant force; F_a , the axial component of the resultant force; F_θ , the component of the resultant force in the tangential direction; and β_m , the angle between the compressor axis and the mean air velocity. Consideration of momentum relations permits the determination of the power input and the power losses and hence the efficiency. The momentum equation in the tangential direction gives

$$\begin{aligned} F_\theta &= (\rho S V_a) (-V_a \Delta w) \\ &= \rho S V_a^2 (-\Delta w) \end{aligned} \quad (1)$$

which applies equally well to frictional and frictionless flow. This conclusion, however, depends on the assumption that the shear forces along the cylindrical surfaces are negligible and will obviously not be valid in the boundary-layer region near the hub and casing. Where these shear forces are appreciable it is not possible to treat the blade elements as independent. It appears, however, that these shear forces can be neglected except near the annular-passage walls where the present theory does not apply. The power input of the row of B_R rotor blades per unit blade length is given by

$$P_I = B_R F_{\theta,R} U \quad (2)$$

The power loss in a row of blades may be obtained by considering the momentum equation in the direction of V_m

$$(p_2 - p_1)S \cos \beta_m = (\rho V_a S) V_a (-\Delta w) \sin \beta_m - D \quad (3)$$

The effect of drag is a loss in pressure rise. The power loss in the annulus per unit blade length is given by

$$P_L = (\Delta p_{id} - \Delta p) V_m B S \cos \beta_m \quad (4)$$

where Δp_{id} is the ideal pressure rise for frictionless flow, Δp the actual pressure rise, and $V_m B S \cos \beta$ the volume rate of flow in the elementary annulus per unit blade length. From equations (3) and (4) it is evident that the power loss for the blades of the annulus per unit blade length is given by

$$P_L = BDV_m$$

This power loss may be expressed in terms of the drag-lift ratio D/L and tangential component of the resultant force F_θ as follows:

$$P_L = BL \left(\frac{D}{L} \right) V_m \quad (5)$$

and, from figure 16

$$\begin{aligned} L &= (F_\theta - D \sin \beta_m) \frac{1}{\cos \beta_m} \\ &= \frac{F_\theta}{\cos \beta_m} - L \left(\frac{D}{L} \right) \tan \beta_m \end{aligned}$$

or by solving for L

$$L = \frac{F_\theta}{\cos \beta_m \left[1 + \left(\frac{D}{L} \right) \tan \beta_m \right]} \quad (6)$$

From equations (5) and (6)

$$P_L = \frac{\left(\frac{D}{L} \right) V_m F_\theta B}{\cos \beta_m \left[1 + \left(\frac{D}{L} \right) \tan \beta_m \right]} \quad (7)$$

This equation applies to either rotor or stator blades when the values of the variable appropriate to the particular blade row are used. The total power loss for a stage is therefore given by

$$\begin{aligned} P_{L,T} &= \frac{\left(\frac{D}{L} \right)_R V_{m,R} F_{\theta,R} B_R}{\cos \beta_{m,R} \left[1 + \left(\frac{D}{L} \right)_R \tan \beta_{m,R} \right]} \\ &\quad + \frac{\left(\frac{D}{L} \right)_S V_{m,S} F_{\theta,S} B_S}{\cos \beta_{m,S} \left[1 + \left(\frac{D}{L} \right)_S \tan \beta_{m,S} \right]} \end{aligned} \quad (8)$$

The loss ratio ζ , which is equal to $1 - \eta$ where η is the blade-element efficiency of the stage, is obtained by dividing the total power loss by the power input as given by equation (2). The quantity $F_{\theta,S} B_S$ may be eliminated by the relation

$$\frac{F_{\theta,S} B_S}{F_{\theta,R} B_R} = \frac{\Delta w_S}{\Delta w_R} \quad (9)$$

which is obtained by multiplying equation (1) by B and noting that SB equal to $2\pi r$ is the same for the rotor and stator blades. If equation (8) is divided by equation (2) and $F_{\theta,S} B_S$ is eliminated by equation (9) with the assumption that Δw_R equals Δw_S as is usually the case for design conditions, the loss ratio is obtained

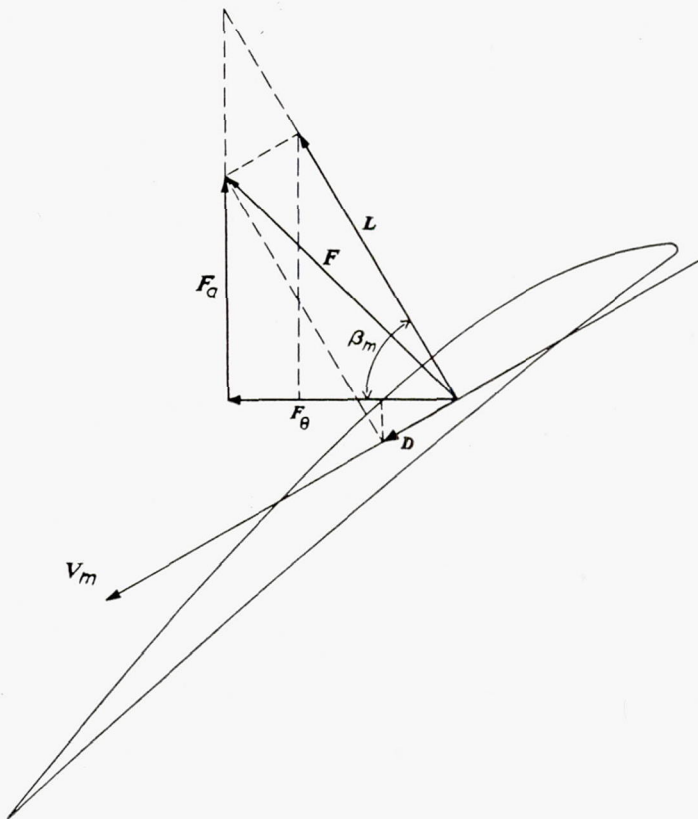


FIGURE 16.—Aerodynamic forces acting on blade element.

$$\xi = \frac{\left(\frac{D}{L}\right)_R \left(\frac{V_{m,R}}{U}\right)}{\cos \beta_{m,R} \left[1 + \left(\frac{D}{L}\right)_R \tan \beta_{m,R}\right]} + \frac{\left(\frac{D}{L}\right)_S \left(\frac{V_{m,S}}{U}\right)}{\cos \beta_{m,S} \left[1 + \left(\frac{D}{L}\right)_S \tan \beta_{m,S}\right]} \quad (10)$$

This relation can be conveniently expressed in terms of the velocity ratios u and w_m (fig. 15 (b)) by noting that

$$\cos \beta_m = \frac{1}{\sqrt{1+w_m^2}}$$

$$\tan \beta_m = w_m$$

$$\frac{V_m}{U} = \frac{V_m}{V_a} \frac{V_a}{U} = \frac{\sqrt{1+w_m^2}}{u}$$

Thus

$$\xi = \frac{\left(\frac{D}{L}\right) (1+w_{m,R}^2)}{u \left[1 + \left(\frac{D}{L}\right)_R w_{m,R}\right]} + \frac{\left(\frac{D}{L}\right)_S (1+w_{m,S}^2)}{u \left[1 + \left(\frac{D}{L}\right)_S w_{m,S}\right]} \quad (11)$$

The value of D/L is of the order of 0.05 and for the normal values of w_m , the terms $(D/L)_R w_{m,R}$ and $(D/L)_S w_{m,S}$ in the denominators can be neglected without appreciable error. Although D/L will, in general, slightly vary with β_m , this variation will depend upon many factors such as solidity, blade section, lift coefficient, etc. Inasmuch as no general relation is known for this variation, D/L will be assumed constant and the same for the rotor and stator blades. With these approximations and with $u - w_{m,S}$ substituted for $w_{m,R}$, equation (11) becomes

$$\begin{aligned} \xi &= \frac{D}{L} \left[\frac{2}{u} + \frac{(u-w_{m,S})^2}{u} + \frac{w_{m,S}^2}{u} \right] \\ &= \frac{D}{L} \left(\frac{2+2w_{m,S}^2}{u} + u - 2w_{m,S} \right) \end{aligned} \quad (12)$$

The minimum value of ξ is obtained by differentiating equation (12) with respect to u and $w_{m,S}$ and setting the derivatives equal to zero,

$$\frac{\partial \xi}{\partial u} = \frac{D}{L} \left(-\frac{2+2w_{m,S}^2}{u^2} + 1 \right) = 0 \quad (13)$$

$$\frac{\partial \xi}{\partial w_{m,S}} = \frac{D}{L} \left(\frac{4w_{m,S}}{u} - 2 \right) = 0 \quad (14)$$

From these equations are obtained

$$w_{m,S} = \frac{u}{2} \quad (15)$$

and

$$u = 2 \quad (16)$$

The condition $w_{m,S} = u/2$ shows that the minimum losses are obtained with a symmetrical velocity diagram. For a symmetrical velocity diagram

$$\xi = \frac{D}{L} \left(\frac{2}{u} - \frac{u}{2} \right) \quad (17)$$

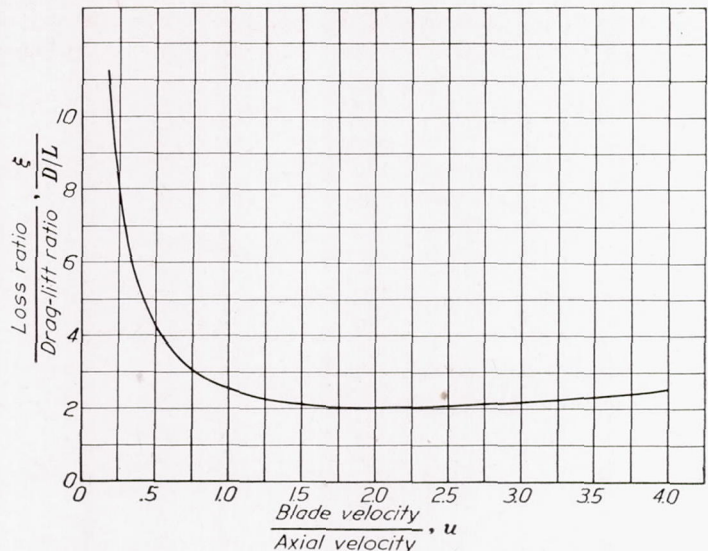


FIGURE 17.—Blade-profile losses in single stage for symmetrical velocity diagram.

Figure 17 shows $\xi / D/L$ plotted against u . Good efficiencies are obviously attainable with a symmetrical velocity diagram over a fairly wide range of values of u . When $u=2$

$$\xi_{min} = 2 \frac{D}{L} \quad (18)$$

Near the point of maximum efficiency, the effect of neglecting the terms $(D/L)_R w_{m,R}$ and $(D/L)_S w_{m,S}$ is small; for $D/L=0.05$ the error in ξ is about 5 percent corresponding to an error in η of about 0.5 percent. If these terms are included, however, the value of u for minimum losses will be slightly increased. For high solidities a slight shift in the opposite direction in the value of u for minimum losses may result from the increase in the value of D/L with β_m that is indicated by the cascade tests of Shimoyama (reference 18).

Inasmuch as all the useful energy put into the air goes into a rise in pressure, the useful power per unit blade length is, for small pressure changes, given by

$$P_u = \eta \rho 2 \pi r V_a^3 u (-\Delta w)$$

$$= 2 \pi r V_a \Delta p$$

and therefore

$$\Delta p = \eta \rho V_a^2 u (-\Delta w) \quad (19)$$

is the pressure rise in a single stage.

DESIGN OF SINGLE STAGE OF COMPRESSOR

In the design of a single stage, the axial velocity is assumed constant with respect to the radius. The lift coefficient C_L is defined in a manner similar to that for isolated airfoils with the mean relative velocity V_m replacing the free-stream velocity

$$C_L = \frac{L}{\frac{1}{2} \rho V_m^2 c} \quad (20)$$

The substitution of L and F_θ from equations (6) and (1) in equation (20) gives

$$C_L = \frac{\rho S V_a^2 (-\Delta w)}{\frac{1}{2} \rho V_m^2 c \cos \beta_m [1 + (D/L) \tan \beta_m]} \quad (21)$$

If this equation is expressed in terms of the velocity ratios u , w_m , and Δw ,

$$C_L \sigma = \frac{2(-\Delta w)}{\sqrt{1+w_m^2} [1+(D/L)w_m]} \quad (21)$$

where σ is the solidity $\frac{c}{S} = \frac{cB}{2\pi r}$. If the term $(D/L)w_m$ is neglected, this equation reduces to

$$C_L \sigma = \frac{2(-\Delta w)}{\sqrt{1+w_m^2}} \quad (22)$$

For a symmetrical velocity diagram, w_m is the same for the rotor and stator and equation (22) becomes

$$C_L \sigma = \frac{2(-\Delta w)}{\sqrt{1+u^2/4}} \quad (23)$$

For the same amount of work to be done per pound of air at the hub as at the tip, it is necessary that

$$u_h |\Delta w_h| = u_t |\Delta w_t|$$

or, because

$$\frac{u_t}{u_h} = \frac{r_t}{r_h}$$

$$|\Delta w_t| = \frac{r_h}{r_t} |\Delta w_h| \quad (24)$$

Inasmuch as u_t is always larger than u_h and, from equation (24), $|\Delta w_h|$ is always larger than $|\Delta w_t|$, equation (23) shows that, for a symmetrical velocity diagram at all radii, the maximum value of $C_L \sigma$ will occur at the hub.

According to Keller (reference 16, p. 48), stalling can be avoided by keeping the solidity (chord-spacing ratio) below 1.1 and the lift coefficient below 1.0. A conservative lift coefficient of 0.7 at the hub was used in the design of the NACA axial-flow compressor. Tests on high-speed airfoils indicate that good efficiencies should be obtained at this lift coefficient (reference 34). Because of the lower lift coefficient used in the design, slightly higher solidities than those recommended by Keller were permitted; solidities at the hub ranged from 1.1 to 1.2.

Reference 34 also illustrates that a practical limit to the speed at which airfoils give good efficiency is about $0.7a$, where a is the velocity of sound. From the velocity diagram

$$V_1^2 = V_a^2 \left[1 + \left(w_m - \frac{\Delta w}{2} \right)^2 \right]$$

or

$$\left(\frac{V_1}{a_1} \right)^2 = 0.49 \left(\frac{V_a}{a_1} \right)^2 \left[1 + \left(w_m - \frac{\Delta w}{2} \right)^2 \right] \quad (25)$$

Equation (25) is a conservative limitation on the maximum allowable axial velocity in a wheel. From inspection of equations (24) and (25), it is evident that this limitation will be imposed at the tip section for the symmetrical case.

NACA AXIAL-FLOW COMPRESSOR

A single stage of the NACA axial-flow compressor was designed by applying the limitation on C_L and σ at the hub and the velocity-of-sound limitation at the tip. A value of

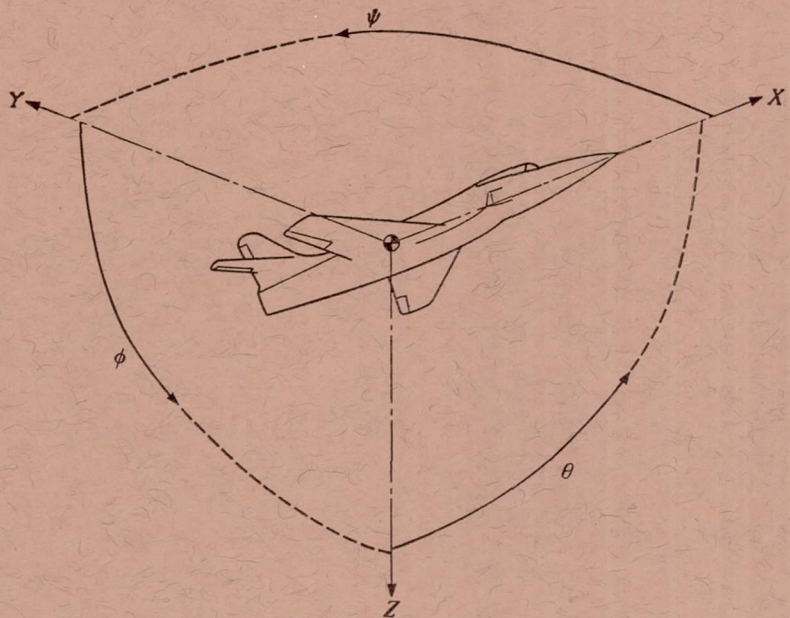
u near the middle of the compressor was initially chosen so as to make the blade elements throughout the compressor operate in the high-efficiency range shown in figure 17. Application of the equation of continuity, together with the hub and the tip conditions for each stage, permitted the completion of the design for all stages.

In order to give the air the amount of rotation specified by the design conditions, the row of entrance guide vanes is quite different in form from the other stationary rows. For the same reason the first rotating blades were given considerably greater twist than the succeeding rotating blades.

REFERENCES

1. Suplee, H. H.: The Gas Turbine. J. B. Lippincott Co., 1910.
2. Meyer, Adolf: The Combustion Gas Turbine: Its History, Development, and Prospects. Proc. Inst. Mech. Eng. (London), vol. 141, May 1939, pp. 197-222.
3. Rettaliata, J. T.: The Gas Turbine. Part I. Allis-Chalmers Electrical Rev., vol. VI, no. 3, Sept. 1941, pp. 20-27.
4. Schmidt, Henry F.: Some Screw Propeller Experiments with Particular Reference to Pumps and Blowers. Jour. Am. Soc. Naval Eng., vol. XL, no. 1, Feb. 1928, pp. 1-26; discussion by Hagen, Jour. Am. Soc. Naval Eng., vol. XL, no. 2, May 1928, pp. 314-319.
5. Christiani, K.: Experimentelle Untersuchung eines Tragflügelprofils bei Gitteranordnung Luftfahrtforschung, Bd. 2, Heft 4, Aug. 27, 1928, pp. 91-110.
6. Harris, R. G., and Fairthorne, R. A.: Wind Tunnel Experiments with Infinite Cascades of Aerofoils. R. & M. No. 1206, British A. R. C., 1928.
7. Numachi, Fukusaburō: Aerofoil Theory of Propeller Turbines and Propeller Pumps with Special Reference to the Effects of Blade Interference upon the Lift and the Cavitation. Tech. Rep., Tōhoku Imperial Univ., vol. 8, no. 3, 1929, pp. 411-469.
8. Troller, Th.: Zur Berechnung von Schraubenventilatoren. Abh. aus dem Aerod. Inst. Tech. H. S. Aachen, Heft 10, 1931, pp. 43-47.
9. Betz, A.: Diagrams for Calculation of Airfoil Lattices. NACA TM No. 1022, 1942.
10. Pfleiderer, C.: Die Kreiselpumpen. Julius Springer (Berlin), 2d ed., 1932, pp. 300-332, 402, and 412-413.
11. Tietjens, O. G.: The Propeller-Type Fan. A. S. M. E. Trans., APM-54-13, vol. 54, no. 13, June 1932, pp. 143-152.
12. Marks, L. S., and Weske, J. R.: The Design and Performance of Axial-Flow Fan. A. S. M. E. Trans., AER-56-13, vol. 56, no. 11, Nov. 1934, pp. 807-813; discussion by C. Keller; R. G. Folsom and M. P. O'Brien; and Alexey J. Stepanoff; A. S. M. E. Trans., vol. 57, no. 6, Aug. 1935, pp. 343-346.
13. von Kármán, Th., and Bergers, J. M.: Flow through a Lattice Composed of Airfoils. Vol. II of Aerodynamic Theory, div. E, ch. II, pt. B, sec. 23, W. F. Durand, ed., Julius Springer (Berlin), 1935, pp. 91-96.
14. Weinig, Fritz: Die Strömung un die Schaufeln von Turbomaschinen. J. A. Barth (Leipzig), 1935.
15. Marks, L. S., and Flint, T.: The Design and Performance of a High-Pressure Axial-Flow Fan. A. S. M. E. Trans., AER-57-1, vol. 57, no. 7, Oct. 1935, pp. 383-388; discussion by C. E. Peck, A. S. M. E. Trans., vol. 58, no. 3, April 1936, pp. 247-248.
16. Keller, Curt, and Marks, L. S.: The Theory and Performance of Axial-Flow Fans. McGraw-Hill Book Co., Inc., 1937.
17. Ruden, P.: Investigation of Single-Stage Axial Fans. NACA TM No. 1062, 1944.
18. Shimoyama, Yoshinori: Experiments on Rows of Aerofoils for Retarded Flow. Trans. Soc. Mech. Eng. (Japan), vol. 3, no. 13, Nov. 1937, pp. 334-344. Text in Japanese, English summary, pp. S-83 and S-84.

19. Pistolesi, E., and Toniolo, A.: Sul Calcolo Practico delle Shiere Alari. *L'Aerotechnica*, vol. XVIII, no. 10, Oct. 1938, pp. 1065-1094.
20. Thompson, L. N.: Propeller-Type Blowers Cool Hell Gate Generators. *Power*, vol. 70, no. 4, July 23, 1929, pp. 127-130.
21. Anon.: Impeller-Blower for Marine Use. *Marine Eng. and Shipping Age*, vol. XXXVII, no. 11, Nov. 1932, pp. 481-482.
22. Richardson, A. S.: Propeller Type Mine Fan at Moose Shaft, Butte, Montana. *Am. Inst. Mining and Metallurgical Eng., Tech. Pub.* no. 484, Feb. 1932, pp. 1-10.
23. Adamchik, M. T.: The Aeroto Forced-Draught Fan. *Engineering*, vol. CXXXI, no. 3413, June 12, 1931, pp. 756-758, and 766; also letter from J. B. McGillivray to the ed., June 19, 1931, p. 804; author's reply, June 26, 1931, pp. 835-836.
24. Keller, C.: Multi-Stage Axial-Flow Fans of Today and Yesterday Design. *Escher Wyss News*, vol. XI, no. 2, April-June 1938, pp. 39-44.
25. The Velox Steam Generator. *Mech. Eng.*, vol. 57, no. 8, Aug. 1935, pp. 469-478.
26. Betz, A.: Axial Blowers. *Air Ministry Trans.* No. 967 (British), 1938.
27. Stodola, A.: Load Tests of a 4000-KW Combustion-Turbine Set. *Engineering*, vol. 149, Jan. 5, 1940, pp. 1-4.
28. Seippel, C.: The Development of the Brown-Boveri Axial Compressor. *The Brown Boveri Rev.*, Brown, Boveri & Co., Ltd. (Switzerland), vol. XXVII, no. 5, May 1940, pp. 108-113.
29. Garrick, I. E.: On the Plane Potential Flow Past a Lattice of Arbitrary Airfoils. *NACA Rep. No. 788*, 1944.
30. Bell, E. Barton: Test of a Single-Stage Axial-Flow Fan. *NACA Rep. No. 729*, 1942.
31. Bell, E. Barton, and DeKoster, Lucas J.: The Effect of Solidity, Blade Section, and Contravane Angle on the Characteristics of an Axial-Flow Fan. *NACA ARR*, Dec. 1942.
32. Bell, E. Barton, and DeKoster, Lucas J.: Test of a Dual-Rotation Axial-Flow Fan. *NACA ARR*, Dec. 1942.
33. Newkirk, Burt L., and Grobel, Lloyd P.: Oil-Film Whirl—Non-whirling Bearing. *A. S. M. E. Trans.*, APM-56-10, vol. 56, no. 8, Aug. 1934, pp. 607-613; discussion, pp. 613-615.
34. Stack, John, and von Doenhoff, Albert E.: Tests of 16 Related Airfoils at High Speeds. *NACA Rep. No. 492*, 1934.
35. Capon, R. S., and Brooke, G. V.: The Application of Dimensional Relationships to Air Compressors, with Special Reference to the Variation of Performance with Inlet Conditions. *R. & M. No. 1336*, British A. R. C., 1930.
36. Goldstein, S.: Modern Developments in Fluid Dynamics. Vol. II. Clarendon Press (Oxford), 1938, p. 449.



Positive directions of axes and angles (forces and moments) are shown by arrows

Axis		Force (parallel to axis) symbol	Moment about axis			Angle		Velocities	
Designation	Symbol		Designation	Symbol	Positive direction	Designation	Symbol	Linear (component along axis)	Angular
Longitudinal.....	X	X	Rolling.....	L	$Y \rightarrow Z$	Roll.....	ϕ	u	p
Lateral.....	Y	Y	Pitching.....	M	$Z \rightarrow X$	Pitch.....	θ	v	q
Normal.....	Z	Z	Yawing.....	N	$X \rightarrow Y$	Yaw.....	ψ	w	r

Absolute coefficients of moment

$$C_l = \frac{L}{qbS} \quad C_m = \frac{M}{qcS} \quad C_n = \frac{N}{qbS}$$

(rolling) (pitching) (yawing)

Angle of set of control surface (relative to neutral position), δ . (Indicate surface by proper subscript.)

4. PROPELLER SYMBOLS

D	Diameter	P	Power, absolute coefficient $C_P = \frac{P}{\rho n^3 D^5}$
p	Geometric pitch		
p/D	Pitch ratio		
V'	Inflow velocity	C_s	Speed-power coefficient = $\sqrt[5]{\frac{\rho V^6}{P n^2}}$
V_s	Slipstream velocity	η	Efficiency
T	Thrust, absolute coefficient $C_T = \frac{T}{\rho n^2 D^4}$	n	Revolutions per second, rps
Q	Torque, absolute coefficient $C_Q = \frac{Q}{\rho n^2 D^5}$	Φ	Effective helix angle = $\tan^{-1} \left(\frac{V}{2\pi r n} \right)$

5. NUMERICAL RELATIONS

$$1 \text{ hp} = 76.04 \text{ kg-m/s} = 550 \text{ ft-lb/sec}$$

1 metric horsepower = 0.9863 hp

$$1 \text{ mph} = 0.4470 \text{ mps}$$

$$1 \text{ mps} = 2.2369 \text{ mph}$$

$$1 \text{ lb} = 0.4536 \text{ kg}$$

$1 \text{ kg} = 2.2046 \text{ lb}$

1 mi = 1,609.35 m = 5,280 ft

1 m = 3.2808 ft.